MODELING POWER GRID RECOVERY AND RESILIENCE POST EXTREME WEATHER EVENTS

by

Priyadharshini Kumaravelan, B.E

A thesis submitted to the Graduate Council of
Texas State University in partial fulfillment
of the requirements for the degree of
Master of Science
with a Major in Electrical Engineering
December 2019

Committee Members:

Tongdan Jin, Chair

Clara Novoa

Dincer Konur

FAIR USE AND AUTHOR'S PERMISSION STATEMENT

Fair Use

Duplication Permission

DEDICATION

I must express my very profound gratitude to my husband, my parents and family for providing me with unparalleled support and continuous encouragement throughout my years of study and through the process of researching and writing this thesis. This accomplishment would not have been possible without them.

ACKNOWLEDGEMENTS

I would like to thank my thesis advisor, Dr. Tongdan Jin, in the Ingram School of Engineering at Texas State University for all his endless support in guiding me in my research and giving me valuable advice. He has always been there to support and give helpful guidance whenever I needed his help.

I would also like to thank Dr. Clara Novoa in the Ingram School of Engineering at Texas State University who is always there to provide insightful help and support. I would like to extend my gratitude to her for advising me in enhancing my research capabilities.

I would also like to thank Dr. Dincer Konur in the McCoy College of Business Administration at Texas State University who is always there to guide the research from a business perspective.

I would also like to thank all the professors and staff of the Ingram School of Engineering at Texas State University in extending their guidance throughout my school years. Last but not least, I would express my gratitude to the National Science Foundation for supporting my thesis project under the NSF Environmental Sustainability ME-GREEN Grant (#1704933).

TABLE OF CONTENTS

Page

ACKNOWLEDGEMENTS v

LIST OF TABLES ix

LIST OF FIGURES xi

LIST OF ABBREVIATIONS xiv

ABSTRACT xv

CHAPTER

1. INTRODUCTION AND LITERATURE REVIEW 1

    1.1 Introduction 1
    1.2 Resilience of power system 2
    1.3 Resilience Enhancement in Power System 4
    1.4 Resilience Enhancement in the Design Phase of Power Grid 6
    1.5 Resilience Enhancement in the Operation Phase of Power Grid 8
    1.6 Resilience Enhancement in the Recovery Phase of Power Grid 9

2. MODELING EXTREME EVENTS 15

    2.1 Modeling a Hurricane 15
        2.1.1 Introduction 15
        2.1.2 Annual occurrence 16
        2.1.3 Approach angle 17
        2.1.4 Translation velocity 18
        2.1.5 Central pressure difference 19
        2.1.6 Radius to maximum wind speed 21
        2.1.7 Wind speed decay rate 21
        2.1.8 Central pressure filling rate 21
        2.1.9 Hurricane intensity measurement 22
        2.1.10 Sample Hurricane simulation 22
    2.2 Modeling a Flood 24
    2.3 Modeling an Earthquake 27
        2.3.1 Introduction 27

2.3.2 Occurrence of an earthquake 28
2.3.3 Magnitude of an earthquake....29
2.3.4 Intensity of an earthquake....30
2.3.5 Hazard Maps 32

3. REPAIR AND RECOVERY MODEL OF POWER LINES 34

3.1 Operation of Power Grid System....34
3.2 Power System Components 36
3.3 The Recovery Model of Transmission and Distribution Lines....37
3.4 Application to Hurricane Harvey....39
3.5 Sensitivity Analysis and Results....44
3.5.1 Effect of repair rate on L, W and W_q 44
3.5.2 Effect of failure rate on L and W....45
3.5.3 Effect of number of repair teams on L, L_q, W and W_q....46
3.5.4 Effect of K on number of repair teams....47

4. ELECTRIC VEHICLES FOR ATTAINING GRID RESILIENCE....49

4.1 Battery swap station....49
4.2 Modeling Electric Vehicle battery swap processes 50
4.3 Optimizing the number of spare batteries for various EV models....52
4.4 Results and Discussions....55
4.5 Calculating the Energy and Power available from an EV 58

5. ENHANCING RESILIENCE OF INDUSTRIAL FACILITY THROUGH VEHICLE TO GRID OPERATION....61

5.1 Using EV for Vehicle-to-Grid Operations in extreme weather 61
5.2 Enhancing Power Resilience of Industrial Facility through V2G Operations....62
5.2.1 Model setting 62
5.3 Model to calculate the cost under normal condition....64
5.4 Results and Observations....65
5.4.1 Effect of battery capacity cost on the system....66
5.4.2 Effect of PV capacity cost on the system....67
5.5 Model to calculate the cost under Extreme Weather Event....68
5.6 Result Analysis and Discussion....71
5.6.1 Effect of EV fleet size on the cost 71
5.6.2 Effect of production loss due to power shortage 72

5.6.3 Effect of V2G service cost 73
5.7 Total Annual System Cost 74

6. CONCLUSION AND FUTURE WORK 76

APPENDIX SECTION 80

REFERENCES 94

LIST OF TABLES

Table **Page**

1. Power grid hardening measures 6

2. Literature review for grid resilience improvement in various phases 14

3. Saffir Simpson Scale 22

4. Hurricane parameters and values 23

5. Sample hurricane simulation results 24

6. Storm Surge for different hurricane Category 25

7. Underground equipment failure rate wrt. hurricane and storm surge 26

8. Energy Released for Various Earthquake Magnitudes 29

9. Modified Mercalli Intensity Scale 30

10. Average cost of one-hour power disruption in the US 34

11. Table of Notation for repair and recovery model of transmission lines 38

12. Transmission line outage data for Hurricane Harvey 42

13. Transmission line recovery data for Hurricane Harvey 43

14. Charging Topologies 52

15. Tesla Supercharger Technology 53

16. Battery capacity of various EV models in the market 53

17. Charging rate of EVs wrt. various charging levels 54

18. Probability of blocking for various levels of charging 57

19. Energy available to AC Loads for various car models 60

20. Notation for calculating cost under normal condition 64

21. Parameter values for normal operating condition.....65

22. Parameters for calculating cost under extreme weather condition 69

23. Parameter values for Extreme Event Condition.....71

24. The values of LCOE in various scenarios.....75

LIST OF FIGURES

Figure **Page**

1. 16-billion-dollar weather and climate disasters in USA in 2017 1
2. Billion-dollar weather and climate disaster frequency mapping 2
3. Resilience curve of a power system 3
4. Aftermath of Hurricane Maria 4
5. Aftermath of Hurricane Harvey 4
6. Damage of distribution towers due to Hurricane Maria 5
7. Resilience improvement strategies 5
8. Use of EVs to power critical load during emergency 11
9. Probability mass function of a Poisson distribution 17
10. Probability mass function of a lognormal distribution 19
11. Probability mass function of a Weibull distribution 20
12. Graphical representation of underground failure rate for data in Table 7 26
13. Flood risk map of the United States 27
14. Seismic Hazard Map of the United States 33
15. North American Bulk Power System 35
16. Typical power grid system 36
17. Markov Transition diagram for recovery of power lines 38
18. Hurricane Harvey's track 40

19. Damaged distribution line....41
20. Flooded substation....41
21. 345 KV line structures down....41
22. Recovery operations post Harvey....41
23. Broken wooden pole....41
24. Recovery post floods from Harvey....41
25. Hurricane Harvey Transmission line outage/return data....42
26. Repair rate versus expected no. of failed lines (L)....44
27. Repair rate versus the expected recovery time (W)....44
28. L versus failure rate....45
29. W versus failure rate....46
30. L, L_q versus repair rate....47
31. W, W_q versus repair teams....47
32. K versus repair teams....48
33. Birth-death process of an Erlang B queuing system....50
34. The minimum s under Level 2 charging with 1% blocking probability....55
35. The minimum s under Level 3 charging with 1% blocking probability....55
36. The minimum s for supercharger for 1% blocking probability....56
37. Spare battery requirement for Level 2 charging....57
38. Spare battery requirement for Level 3 charging....58
39. Spare battery requirement for supercharger....58

40. PEV sale in the US in 2018.....62

41. Microgrid set-up of an industrial facility.....63

42. BSS capacity cost versus system cost - case I.....66

43. BSS capacity cost versus system cost - case II.....67

44. PV capacity cost versus system cost.....67

45. PV and BSS capacity cost versus system cost.....68

46. EV fleet size versus LCOE during extreme event.....72

47. Production loss versus LCOE during extreme event.....73

48. V2G service cost versus LCOE during extreme event.....74

LIST OF ABBREVIATIONS

Abbreviation	Description
BEV	Battery Electric Vehicle
BPU	Board of Public Utilities
BSS	Battery Storage Systems
DAD	Defender-Attacker-Defender
DER	Distributed Energy Resources
DG	Distributed Generation
DPGS	Distributed Power Generation Systems
ERCOT	Electric Reliability Council of Texas
ESS	Energy Storage Systems
EV	Electric Vehicle
FCFS	First Come First Served
FEMA	Federal Emergency Management Agency
HEV	Hybrid Electric Vehicle
HILP	High Impact Low Probability
IPT	Induction Power Transfer
LCOE	Levelized Cost of Electricity (or Energy)
NERC	North American Electric Reliability Council
PEV	Plug in Electric Vehicle
PGA	Peak Ground Acceleration
PHEV	Plug in Hybrid Electric Vehicle
PV	Photovoltaic
SDN	Software Defined Networking
TSO	Transmission System Operator
UPFC	Unified Power Flow Controllers
USGS	United States Geological Survey
V2G	Vehicle-To-Grid
V2H	Vehicle-To-Home
VPP	Virtual Power Plant
WT	Wind Turbine

ABSTRACT

The traditional N-1 power grid system is inadequate as it cannot withstand extreme weather events like hurricane, flooding, earthquake etc. Extreme event analysis reports by NERC, BPU, and ERCOT state that failure of outdoor grid components like distribution lines, transformers and generators lead to majority of the power outages where millions of customers get affected. This research addresses the problem of power grid resilience post an extreme weather event and how the grid recovery can be planned and executed. We propose a repair and recovery model for transmission lines for the case of Hurricane Harvey and analyze how the repair rate and the failure rate affect various performance metrics. We analyze how electric vehicles (EV) can be used as a potential alternative to build resilience of a power system in contingency. A mathematical model is developed for the EV battery swap process and the minimum spare battery requirement is analyzed for various scenarios. We present a Vehicle-to-Grid (V2G) based resilience model for critical loads like manufacturing facility during an extreme event. The main goal of this model is to determine the sizing and siting of the wind- and solar-based microgrid to ensure power resilience through island operations. Through this model, we analyze how the number of EVs, battery capacities, industrial production loss and the V2G service cost affect the levelized cost of energy (LCOE) in extreme weather condition.

1. INTRODUCTION AND LITERATURE REVIEW

1.1 Introduction

Electrical power systems are critical infrastructure of our society because they support economic, business and social activities in everyday life. They must be reliable during normal conditions and also be resilient to high-impact low-probability (HILP) events. Despite low probability, severe weather events like hurricane, earthquake, and snowstorm often have dramatic consequences on power systems, affecting the operation and reliability of outdoor components like transmission towers and overhead lines. In 2017, the USA was affected by 16 separate billion dollar disaster events which include three tropical cyclones, eight severe storms, two inland floods, one crop freeze, one drought and one wildfire (Smith et al. 2018).

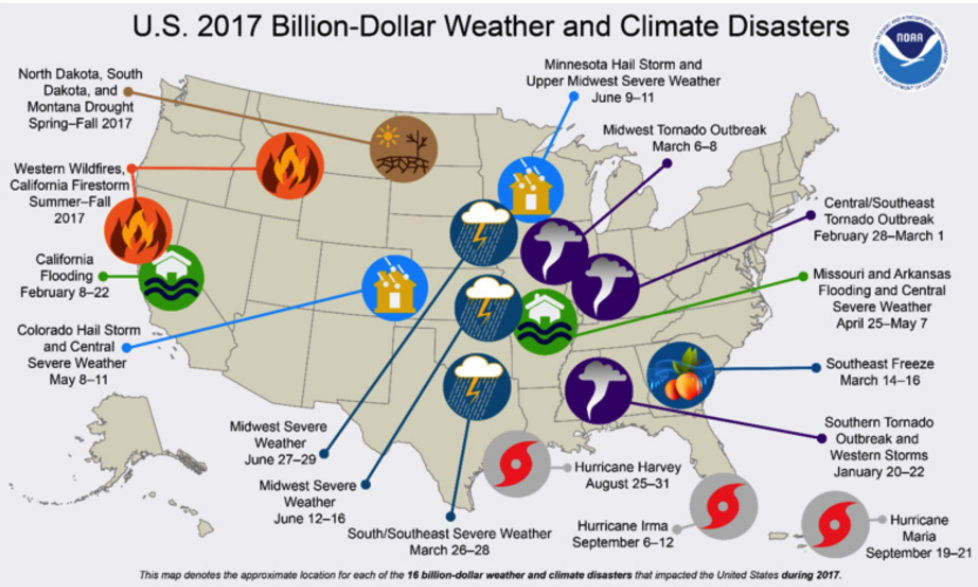

Figure 1. 16-billion-dollar weather and climate disasters in the USA in 2017(Smith et al. 2018)

Among all these extreme weather events, those that left ineradicable impact are hurricanes Irma, Maria, Harvey and the California firestorm.

The following figure shows the geography of billion-dollar disaster events by type from 1989 to 2017 in the USA.

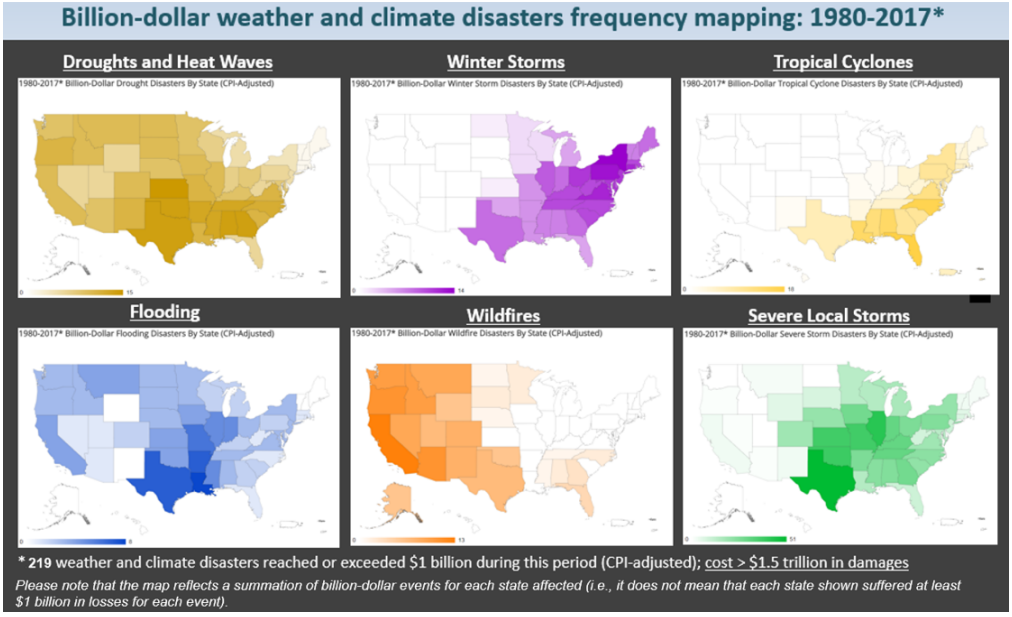

Figure 2. Billion-dollar weather and climate disaster frequency mapping (Smith et al. 2018)

1.2. Resilience of a power system

Extreme weather events have dramatic impacts on the resilience of a power system. Resilience is derived from the Latin word “resilio” which literally refers to the ability of an object to rebound or return to its original shape or position after being stressed. Resilience with respect to power infrastructure is defined as “the ability of a power system to recover quickly following a disaster or, more generally, to the ability of anticipating extraordinary and high-impact, low-probability events, rapidly recovering from these disruptive events, and absorbing lessons for adapting its operation and structure for preventing or mitigating the impact of similar events in the future” (Panteli et al. 2015). Figure 3 shows the conceptual resilience curve of a power system.

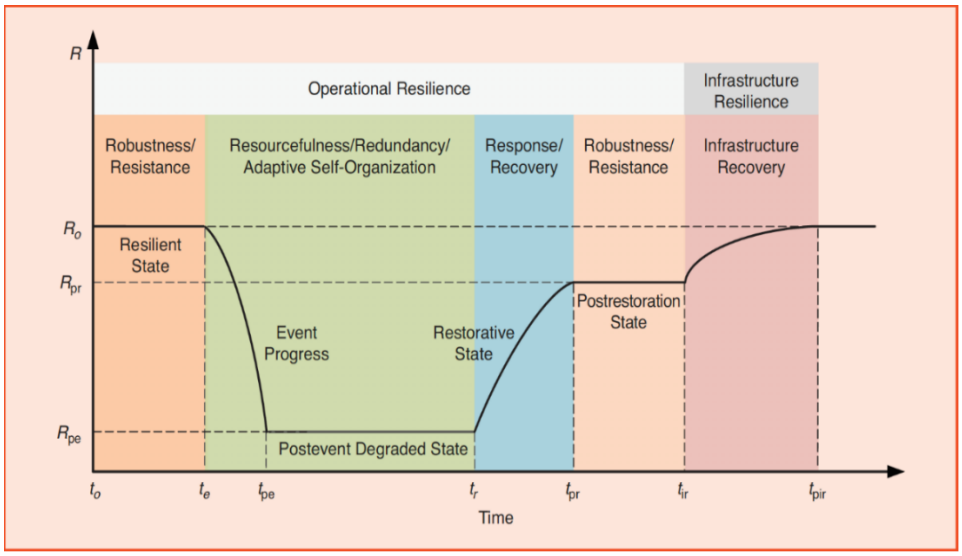

Figure 3. Resilience curve of a power system (Panteli et al. 2015)

Figure 3 shows how the resilience of a power system as a function of time gets affected with respect to an extreme event. Robustness and resistance are considered as the key resilient features for a system before an extreme event occurs at t_e. After the event has occurred, the resilience of the system drops from R_o to R_{pe} and the system enters the post event degraded state. Note that both R_o to R_{pe} represent the system performance index, such as power delivered, or energy supplied. Resourcefulness, redundancy and adaptive self-organization play a key role in the system survival in this state. After this stage, the system enters the restorative state. In this state, the system should be able to heal itself and return to its normal state as quickly as possible. Now the system enters the post restoration state with a resilience level R_{pr} which might or might not be the same as the pre-event resilience level R_o. However, if the system's components are damaged extensively due to an extreme weather event like hurricane, the system might not demonstrate sufficient resilience in performance. Rather it may take longer for the system to return to its original state as it can be seen in Figure 3.

1.3 Resilience Enhancement in Power Systems

Power systems should be able to withstand unanticipated catastrophic events, climate change and man-made incidents. When Maria, a Category 4 hurricane, stormed into Puerto Rico, it damaged almost 80% of the island's grid and 40% of the 334 substations suffered major damages (Gallucci, 2018). The following figures show how the critical infrastructures of a power system such as the transmission towers, and distribution poles and lines have been damaged due to hurricanes.

Figure 4. Aftermath of Hurricane Maria (Fortune,2017)

Figure 5. Aftermath of Hurricane Harvey (Catholic Sun, 2017)

Figure 6. Damage of distribution towers due to Hurricane Maria (Electric Light and Power, 2018)

In this research we are going to address the problem of resilience in four different aspects as shown in Figure 7 below.

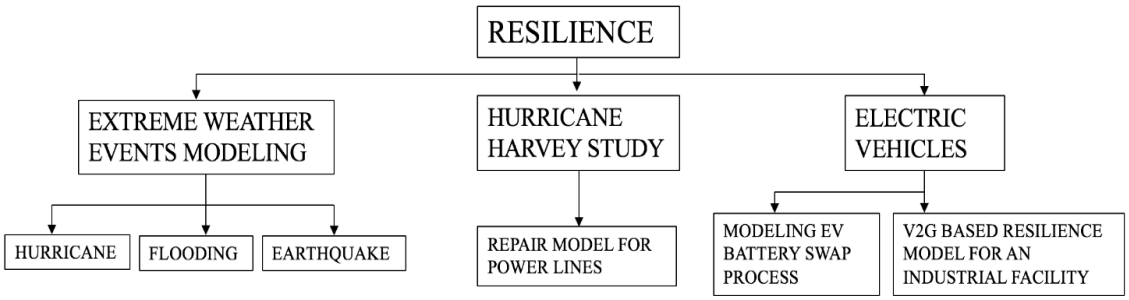

Figure 7. Resilience improvement strategies

To begin with we discuss how extreme weather events damage the bulk power system and affects the power grid resilience. We develop mathematical models for some of the extreme weather events, namely hurricane, floods and earthquake. Secondly, we develop a repair and recovery model for transmission lines for the case of Hurricane Harvey and perform sensitivity analysis to see how the repair rate and the failure rate affect various

performance metrics. Thirdly, we discuss how Electric Vehicles (EVs) could be a potential source of power storage and how they can be used to attain grid resilience post the disaster event. Finally, we present an EV based V2G model for an industrial facility and analyze how different factors such as production loss and EV fleet size affect the total system cost.

In order to improve the resilience of an electric power system, proactive measures and resilient techniques can be adopted and implemented in various stages, including the grid design, the operation and the recovery phase. Each of these are discussed in detail in the following sections.

1.4 Resilience Enhancement in the Design Phase of Power Grid

Some of the most common hardening measures are listed in Table 1 below, including modern control measures and protections against flooding and windstorms.

Table 1. Power grid hardening measures (Wang et al., 2016)

Hardening	Activities
Flood Protection	• Elevating structures such as substations, control rooms, and pump stations • Relocating/constructing new lines and facilities • Adding redundant lines to the existing system • Using redundant generating units as backup power
Wind Protection	• Upgrading damaged structures with stronger materials • Strengthening or upgrading poles • Burying power lines underground • Vegetation management
Modernization	• Deploying sensors and control technology • Installing assets such as database or software tools

One of the most common measures for improving the power system resilience is called hardening. It refers to any structural enhancement or topology upgrade in order to make a power system less vulnerable to extreme events. However, hardening might not always provide an optimum solution, partly because it usually involves a significant amount of financial investment on critical power system infrastructure, and partly because it is resource intensive and time consuming for implementation. Some of the measures that are taken to improve the grid resilience in the design stage include the following.

- Hardening measures as discussed in Table 1
- Replacing radial distribution lines with ring configuration
- Redundancy allocation of electrical components, such as generators and overhead transmission lines.
- Placement of backup generating units
- Renewable energy (i.e. WT and PV) integration
- Distributed generation allocation
- Usage of energy storage units including electric vehicle (EV)
- Pro-active resource allocation

Seiver et al. (2007) demonstrate in their study how unified power flow controllers (UPFCs) can be used to reduce cascading outages in a power system transmission line. A cascading failure is a process in a system of interconnected parts in which the failure of one or certain parts can trigger the failure of other parts sequentially. Cascading failure is common in power grids when one of the elements fails (completely or partially) and shifts its load to nearby elements in the system. UPFCs can also be used to find out

critical weakness in a power grid and help fix them. Babaei et al. (2017) propose a 3-level defender-attacker-defender (DAD) framework for line hardening and show how distributed generation (DGs) allocation helps to enhance the distribution power resilience under extreme natural events. Arab et al. (2015) propose an efficient framework for pro-active resource allocation for a power system whose components lie in the path of an upcoming hurricane in order to minimize the costs associated with load interruption, restoration operation and electricity generation. Ma et al. (2018) propose an optimal hardening strategy which involves different strengthening techniques such as upgrading poles and vegetation management in order to minimize the investment cost.

1.5 Resilience Enhancement in the Operation Phase of Power Grid

Works have been done to demonstrate several effective ways to increase resilience of a power system during its operation phase. These measures can be broadly categorized into the following.

- Maintenance and asset management such as condition monitoring, performance-based service contracting, and sensor-driven replacement.
- Vegetation management.
- Periodically replacement of aging units or circuits.
- Islanding schemes to minimize power interruption
- Using Unified Power Flow Controllers (UPFCs)
- Islanded microgrids, and interconnected microgrids
- Virtual power plant operations

Kuntz et al. (2002) propose a maintenance scheduling algorithm based on vegetation failure rate model in order to find the optimal time and location for performing maintenance on overhead distribution feeders. Jahromi et al. (2009) propose a methodology for cost effective maintenance of overhead power distribution lines by utilizing the decoupled risk factors model. Panteli et al. (2016) propose a methodology to boost the power grid resilience based on fragility curves model for windstorms on transmission lines. Their work aims at splitting the grid into self-adequate defensive islands such that components with higher failure probability are isolated, otherwise it might lead to cascading failure effects. Dehghanian et al. (2017) show how topology control (network reconfiguration) can be used to improve grid resilience and perform the forecasting of contingency events.

1.6 Resilience Enhancement in the Recovery Phase of Power Grid

After an extreme event has occurred, it is necessary for the power system to recover and return to its normal state of operation as quickly as possible. Some of the measures that are taken to improve the grid resilience in recovery phase include the following:

- Fast deployment of repair logistics for prompt recovery
- Usage of mobile and backup power resources like diesel engine, mobile generators, mobile transformers, and backup energy storage systems
- Distributed generation like wind- and solar-based microgrid operation
- Vehicle-to-Grid (V2G), and Vehicle-to-Home (V2H) operations
- Reconfiguration of network topology to minimize load outages and to ensure uninterrupted power supply to critical consumers, such as banks, hospital and traffic lights.

Following an extreme weather event, the repair crew should be promptly deployed to assess the damages to a power grid and take initiatives to replace or repair the failed components and circuits. Quite often trees that have fallen and flooded zones served as a major hindrance for repair crews to reach the damaged areas after hurricane Harvey (ERCOT, 2017).

Chester et al. (2015) propose the idea of increasing the resilience of a power system after a disaster attack through onsite wind and solar generation to ensure grid survivability. They also developed a queueing framework to accelerate the recovery process of damaged lines using the machine-repairman model. Mathew et al. (2016) demonstrate in their paper how a microgrid based restoration approach helps in improving the resilience of a power system using automated distributed restoration algorithm and modified spanning tree approach for changing the network topology. Liu et al. (2017) demonstrate how power grids with integrated microgrids help improve power resilience using Markov chain and Monte Carlo simulation technique. Clements et al. (2017) propose a methodology using fragility curves to estimate the impact of wind storms on network resilience and how different staff resource levels can change the impact. Panteli et al. (2017) define the concept of resilience trapezoid which is an extension of the traditional resilience triangle in their paper and discuss different structural and operational resilience enhancement strategies under single and multiple windstorms. Landegren et al. (2016) propose an approach to assess how decision variables related to the technical network and the repair system that comprise of repair resources and prioritization rules for repair impact a system resilience. The repair system here uses queuing model and holds a backup power.

The number of plug-in hybrid electric vehicles (PHEVs) and electric vehicles (EVs) is on the rise due to various reasons such as depleting fossil fuels, air pollution and to have a higher energy efficiency. A PHEV is a hybrid electric vehicle that has a mix of battery storage system and gasoline engine. When the vehicle is charged through an external electric power source, no consumption of gasoline is required. An EV contains a battery pack instead of an internal combustion engine and is propelled by an electric motor. The PHEVs and the EVs are commonly referred to as Plug-in Electric Vehicles (PEVs). Recent technological advancements have made it feasible to use these electric vehicles as energy resources where they inject power into the grid by discharging the battery for a short duration of time (Mohagheghi et al., 2012). This service is referred to as Vehicle-to-Grid (V2G) operation and can aid the grid in various ways including but not limited to serving as a backup power resource, frequency regulation, peak load shaving and smoothing generation from renewable energy resources. In Figure 7 electric vehicle fleets can be used to power critical infrastructures like hospitals, schools, and offices during an outage.

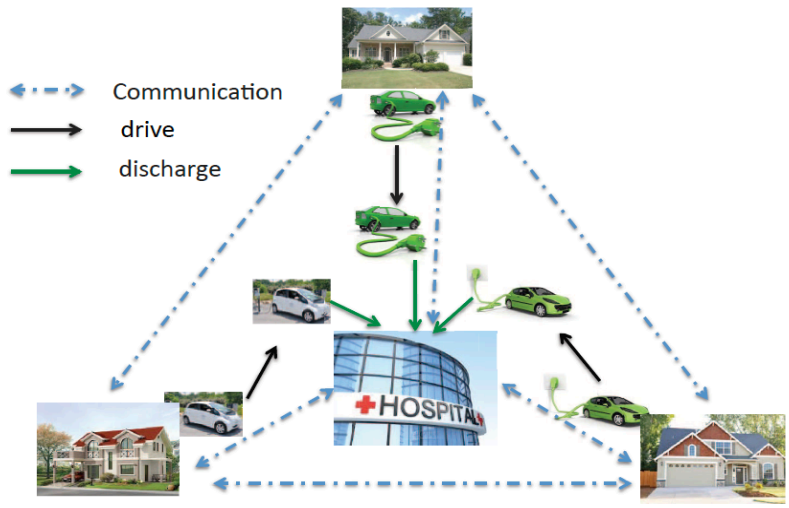

Figure 8. Use of EVs to power critical load during emergency (Maharajan et al. 2015)

Mohagheghi et al. (2012) demonstrate in their study how induction power transfer (IPT) can be used for V2G applications and discuss about the supervisory control of the IPT system. Maharajan et al. (2015) investigate how EVs along with distributed renewable energy resources can be used to improve the resilience of a microgrid and further introduce a software defined networking (SDN) platform for Virtual Power Plant (VPP) applications. Gholami et al. (2016) propose an optimization model for scheduling of microgrids to reduce load curtailments utilizing local reserves, storage units and EVs. Shin et al. (2017) propose an optimization model for vehicle-to-home (V2H) operation and an extended system of vehicles-to-homes (Vs2Hs) under the failure of an external grid.

A microgrid is a power system with a cluster of distributed energy resources (DERs) and loads within a small area. Microgrids with DERs like solar and wind serve as promising alternatives to the traditional power generation and distribution systems. One of the main reasons is that after an extreme weather event, a large geographic area is affected and the recovery of the main power grid that spans over the entire affected area may take from days to months and sometimes even a year. When hurricane Sandy struck in October 2012, about 7.5 million consumers lost electric power across 15 states in the United States. Even after the power restorations operations began, nearly 3.7 million consumers were without power after a few days (Che et al., 2014). A few of the other reasons include aging critical infrastructures, communities located remotely and the need for sustainability. There are efforts going on globally to develop renewable energy resources like solar, wind, thermal, hydropower, ocean power, and bioenergy. Among

these technologies, solar and wind are typical resources due to their easy access and technological maturity.

Lainfiesta et al. (2018) present a data-driven approach for integrating solar generation and energy storage systems into an existing microgrid on the Texas A&M University Kingsville campus. Cox et al. (2014) present an architectural method to improve a microgrid resilience and analyze how transactive energy (TE) operations help in increasing grid resilience and recovery. TE can be defined as "a system of economic and control mechanisms that allows the dynamic balance of supply and demand across the entire electrical infrastructure using value as a key operational parameter. Buque et al. (2016) analyze how microgrids with distributed energy resources like the solar energy will help improve the grid resilience in the Mozambican network as the grid is not able to perform well during adverse weather and peak demand. Li et al. (2017) study how networked microgrid can help improve grid resilience and discuss the advantages of using advanced information and communication technologies (ICTs) for distribution systems. Blaabjerg et al. (2017) discuss about DG comprised of wind and PV units, their protection issues and islanding operations and how it improves the grid resilience. Yao et al. (2017) propose an optimal methodology for reconfiguration of radial distribution system topology in the face of major blackouts and test it on a modified 33-bus test system. The following table summarizes the various references for resilience improvement in three different phases.

Table 2. Literature review for grid resilience improvement in various phases

Phases of Power Grid	Literature references
Design Phase	• Seiver et al. (2007) • Arab et al. (2015) • Babaei et al. (2017) • Ma et al. (2018)
Operation Phase	• Kuntz et al. (2002) • Jahromi et al. (2009) • Panteli et al. (2016) • Dehghanian et al. (2017)
Recovery Phase	• Mohagheghi et al. (2012) • Cox et al. (2014) • Chester et al. (2015) • Maharajan et al. (2015) • Landegren et al. (2016) • Gholami et al. (2016) • Mathew et al. (2016) • Buque et al. (2016) • Shin et al. (2017) • Li et al. (2017) • Blaabjerg et al. (2017) • Yao et al. (2017) • Liu et al. (2017) • Clements et al. (2017) • Panteli et al. (2017) • Lainfiesta et al. (2018)

2. MODELING EXTREME EVENTS

2.1. Modeling a Hurricane

2.1.1. Introduction

Critical infrastructure like electrical power systems should be able to withstand wide scale disturbances and be resilient to high impact low probability (HILP) events. Among the extreme events that cause wide scale power disruptions hurricanes account for a major portion. A hurricane or a tropical storm mostly affects coastal regions and the impact might last from a few days up to several months depending on its impact. The area impacted by the event spans for several hundreds of kilometers (Wang et al., 2016). In the year 2017 hurricanes such as Harvey, Maria and Irma caused extensive damage to the critical infrastructures of the US.

There are many ways in which a hurricane can be modeled such as empirical modelling, sampling approach, and statistical modeling using probability distribution functions. The National Hurricane Center (NHC) uses different forecast models that vary in structure and complexity. Dynamic models also known as numerical models require high speed super computers to run and are most complex and expensive (NOAA,2019). A few examples include Florida State Super Ensemble (FSSE), Global Ensemble Forecast System (AEMI).

Statistical models are not as complex as dynamic models but are based on historical data such as storm location and date. Statistical hurricane intensity prediction scheme (SHIP), Logistic growth equation model (LGEM) are a few examples of statistical models. Statistical-dynamical models blend both the above said models.

For an uncertain event probabilistic modeling is the widely used analysis technique (Xu, 2008). Therefore, most of the hurricane parameters are modeled using probability distribution functions. A few of the critical characteristics include the following.

- Annual occurrence
- Approach angle
- Translation velocity
- Central pressure difference
- Radius to maximum wind speed
- Wind speed decay rate
- Central pressure filling rate

2.1.2. Annual occurrence

The annual occurrence is modeled using Poisson distribution. The number of times the hurricane occurs in a given year can be modeled using the following equation.

$$f(h) = \frac{e^{-\lambda}\lambda^{h}}{h!} \tag{2.1}$$

Where

h is the number of landfalls per year, for h=0, 1, 2…

λ is the average number of hurricanes that land in a given year.

We simulate the time between successive hurricane occurrences using exponential inter-arrival time distribution. The equation used to generate a random number with exponential distribution using inverse transform technique is given below and this value represents the hurricane inter-arrival time (t_{hur}).

$$t_{hur} = \frac{-\log(1 - rand())}{\lambda} \tag{2.2}$$

where *rand*() generates a uniform random value between 0 and 1. Figure 9 shows the probability mass function of a Poisson distribution. The horizontal axis is h and the vertical axis is $f(h)$ for various values of λ.

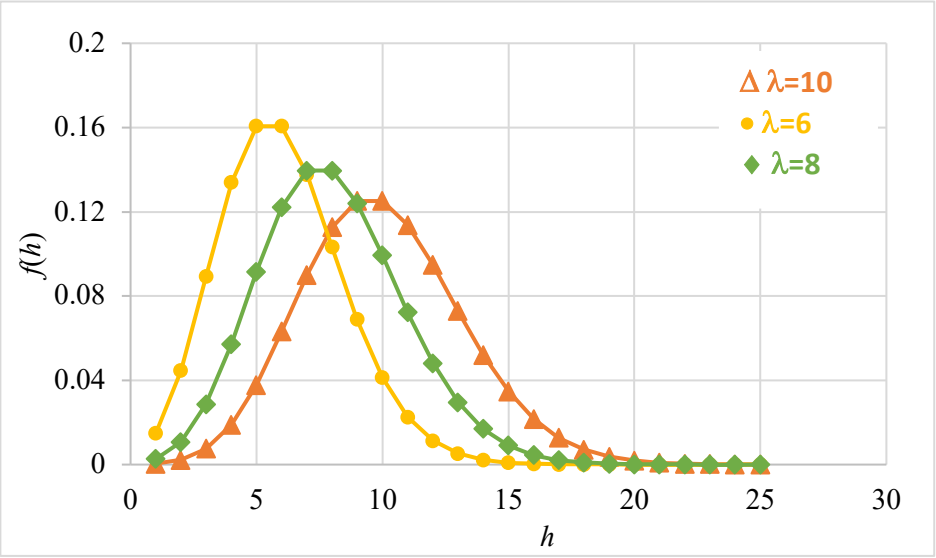

Figure 9. Probability mass function of a Poisson distribution

2.1.3. Approach angle

The approach angle (θ) is modeled using binormal distribution which is a weighted sum of two normal distributions (Xu, 2008). The approach angle indicates the heading direction of a hurricane when it lands on the shore.

$$f(\theta)=\frac{a}{\sigma_{x_1}\sqrt{2\pi}}\exp\left[-\frac{1}{2}\left(\frac{\theta-m_{x_1}}{\sigma_{x_1}}\right)^2\right]+\frac{(1-a)}{\sigma_{x_2}\sqrt{2\pi}}\exp\left[-\frac{1}{2}\left(\frac{\theta-m_{x_2}}{\sigma_{x_2}}\right)^2\right] \quad (2.3)$$

where

m_{x_1}, m_{x_2} are the means of the two normal distributions.

σ_{x_2}, σ_{x_1} are the standard deviation of the two normal distributions.

a is a weighting factor whose value is 0.5.

The equations for calculating the approach angle are given below. Unit for the approach angle is in degrees.

$$\theta_1 = m_{x_1} + \sigma_{x_1} z \tag{2.4}$$

$$\theta_2 = m_{x_2} + \sigma_{x_2} z \tag{2.5}$$

$$\theta = \theta_1 + \theta_2 \tag{2.6}$$

$$z = sin(2\pi rand())\sqrt{-2\,ln(rand())} \tag{2.7}$$

where z is the random value of standard normal distribution.

2.1.4. Translation velocity

The translation velocity indicates the velocity with which the hurricane moves forward after its landfall on the shore. It is modeled using lognormal distribution whose probability density function is given by the following equation.

$$f(c) = \frac{1}{\sigma_{ln(c)} c\sqrt{2\pi}} exp\left[-\frac{1}{2}\left(\frac{ln(c) - m_{ln(c)}}{\sigma_{ln(c)}} \right)^2 \right] \tag{2.8}$$

Where

c is the translation velocity in meters per second (m/s).

$m_{ln(c)}$ is the logarithmic mean.

$\sigma_{ln(c)}$ is the logarithmic standard deviation.

There is a positive correlation between storm approach angle (θ) and the translational velocity c and hence the logarithmic mean is calculated using Equation (2.9) below. The logarithmic standard deviation is treated as a constant (Xu, 2008).

$$m_{ln(c)} = 2.3 - 0.00275\theta \tag{2.9}$$

$$\sigma_{ln(c)} = 0.3 \tag{2.10}$$

The equation to generate a number using lognormal distribution in MATLAB is given below where *logrnd*( ) is a MATLAB function. The random number thus generated here is the translation velocity of the hurricane.

$$c = logrnd\,(m_{ln(c)}, \sigma_{ln\,(c)}) \tag{2.11}$$

Figure 10. shows the probability mass function of a lognormal distribution. The graphs are plotted for various values of σ.

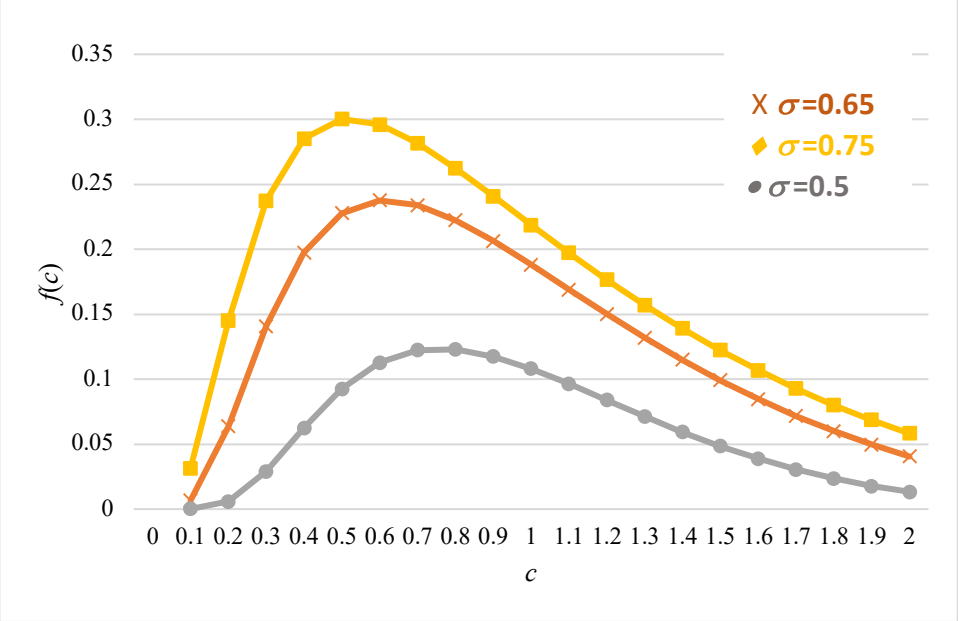

Figure 10. Probability mass function of a lognormal distribution

2.1.5. Central pressure difference

The central pressure difference indicates the gap in pressure at the eye of the hurricane and the atmospheric pressure. It is modeled using Weibull distribution whose PDF is given by the following equation (Xu, 2008).

$$f(\Delta p) = \frac{k}{c}\left(\frac{\Delta p}{c}\right)^{k-1} exp\left[-\left(\frac{\Delta p}{c}\right)^{k}\right] \tag{2.12}$$

Where

Δp is the central pressure difference in millibars.

k is the shape parameter and is a constant whose value is 1.15

c is the scale parameter and is dependent on the approach angle θ.

The formula to generate a value from Weibull distribution is given by the following equation (Vickery et al., 1995). In this case, this value is the central pressure of the hurricane at landing.

$$\Delta p_o = c\log(1-rand())^{1/k} \quad (2.13)$$

where c =35-(0.1θ) and k=1.15, a constant.

The central pressure difference is obtained by subtracting the pressure difference from the atmospheric pressure which is 101.3 Kilopascal (kPa).

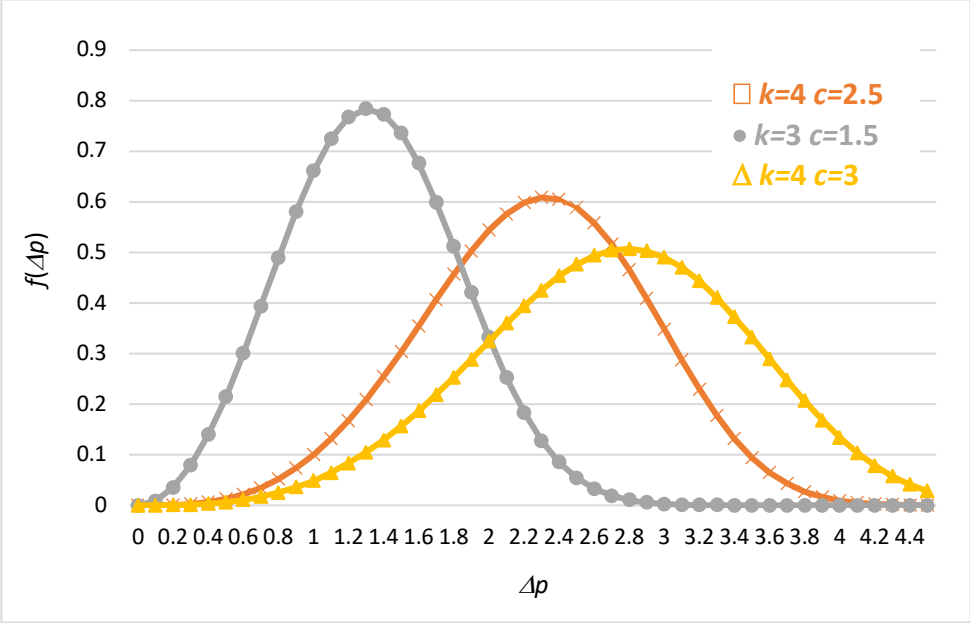

Figure 11. Probability mass function of a Weibull distribution

Figure 11 shows the probability mass function of a Weibull distribution. The graphs are plotted for various values of k and c as indicated in the graph.

2.1.6. Radius to maximum wind speed

The radius to maximum wind speed determines the band where the intensity of the hurricane is the strongest. It is usually measured in kilometer (or km) and is given by the following empirical equation (Xu, 2008).

$$ln\,(R_{max}) = 2.556 - 0.000050255\Delta p^2 + 0.042243032\,\Psi \qquad (2.14)$$

Where

Δp is central pressure difference in millibars

R_{max} is radius of the area in kilometers that has the impact of the hurricane

Ψ is the storm latitude in degrees.

2.1.7. Wind speed decay rate

Once the hurricane lands on the shore, its intensity decays due to land friction and terrain geography. The rate of decay of wind speed is given by the following empirical equation.

$$V(t) = V_b + (RV_0 - V_b)e^{-\alpha t} \qquad (2.15)$$

Where

V_b is the velocity constant whose value is 13.75 m/.

R is the factor of sea land wind speed reduction whose value is 0.9

V_0 is the maximum sustained one-minute surface wind speed at the time of landfall in meters per second.

α is the decay constant whose value is 0.095 per hour.

The wind sped decay rate is simulated for a time period of 72 hours in this research representing a 3-day duration of a storm.

2.1.8. Central pressure filling rate

The central pressure filling rate is given by the following empirical equation.

$$\Delta p(t) = \Delta p_o \, e^{-\alpha t} \tag{2.16}$$

where $$\alpha = 0.006 + (0.00046 \Delta p_o) + 0.025 \tag{2.17}$$

The central pressure is simulated for a time period of 72 hours which is the typical duration of a hurricane event.

2.1.9. Hurricane intensity measurement

In order to measure the hurricane's intensity, a measurement scale known as the Saffir-Simpson scale is used. This scale has a range of 1 to 5 with 1 being the least intensive and 5 being the most intensive hurricane. Table 3 shows the Saffir Simpson scale and how it categorizes hurricanes into different scale based on the minimum central pressure. In general, a lower central pressure implies a stronger or more intensive hurricane.

Table 3. Saffir Simpson Scale (Xu, 2008)

Hurricane Category	Minimum central pressure(mb)
5	<920
4	920-944
3	945-964
2	965-979
1	≥980

2.1.10. Sample Hurricane simulation.

The values for the various parameters of the hurricane characteristics is listed in Table 4. The background of selection of these values are discussed in detail in the work of Xu et al. (2008).

Table 4. Hurricane parameters and values (Xu et al.,2008)

Parameter	Value
Annual Occurrence Rate	
λ	0.29677
Approach angle	
m_{x_1}	35
m_{x_2}	295
σ_{x_1}	25
σ_{x_2}	40
a	0.5
Central Pressure Difference	
K	1.15
Radius to Maximum Wind Speed	
Ψ	25.9°
Maximum wind speed decay rate	
V_b	13.75
R	0.9
α	0.095
V_o	1.287

A sample simulation is executed for a hurricane in MATLAB and the obtained values for its various characteristics is given in Table 5.

As it can be seen from the results, this hurricane falls in Category 1 because the observed central pressure is greater than 980 millibars as per the Saffir-Simpson scale (1 millibar=0.1 KPa). The hurricane has a probability of occurring once in every 5.6 years. The velocity with which the hurricane propagates through the land (translation velocity)

after its landfall is 7.97 m/s. The approach angle is 175.34° (with respect to north) which indicates the angle at which the hurricane will land on the shore. The radius to maximum wind speed is 37.8 km which means that the hurricane's impact can be felt for a radius of 37.8 km surrounding the hurricane eye.

Table 5. Sample hurricane simulation results (mb=millibar)

Parameter	Unit	Value
Annual occurrence rate	events/year	0.176
Approach angle	degree	175.34
Translation velocity	m/s	7.9761
Central pressure difference	mb	17.4753
Central pressure	mb	995.524
Radius to maximum wind speed	km	37.8952

2.2 Modeling a Flood

When a hurricane is about to make a landing, it often causes flooding in the areas near the shore. This is known as storm surge which creates great damage to underground cables, vaults, manholes, etc. Also, the salt residue that is left behind on electrical components like the insulators and bushings after the storm recedes lead to component failure if they are energized.

Table 6 shows the storm surge in meters that would be expected for a given hurricane category. It can be seen from the table below that a Category 5 hurricane has the largest storm surge because it creates the strongest impact when making a landfall (Xu et al., 2008).

Table 6. Storm Surge for different hurricane Category (Xu et al., 2008)

Hurricane Category	Storm Surge (meter)
5	5.5
4	4-5.5
3	2.7-3.7
2	1.8-2.4
1	1.2-1.5

In order to calculate the equipment damage, a mathematical model for the storm surge based on the hurricane category and the storm surge category is proposed by Xu (2008) as follows.

$$\lambda_u = [a + b(H-S)]\, I(H-S) \tag{2.18}$$

where

$$I(H-S) = 1 \text{ for } H-S \geq 0 \text{ and}$$

$$I(H-S) = 0 \text{ for } H-S \leq 0.$$

λ_u is the equipment failure rate. H indicates the hurricane Category from 1 to 5; S is the storm surge Category from 1 to 5; and a and b are tuning parameters. $I(H-S)$ is an indicator function to denote whether a particular area is affected by a hurricane or not.

For example, for a hurricane of Category 3 and a storm surge of Category 2, the equipment failure rate is 6% given a=0.01 and b=0.05. Table 7 shows the equipment failure rate for various hurricane and storm surge categories. Figure 12 shows a three-

dimensional graphical representation of the underground equipment failure rate calculated in Table 7.

Table 7. Underground equipment failure rate wrt. hurricane and storm surge

λ_u		Storm Surge Zone Category				
		1	2	3	4	5
Hurricane Category	1	1%	0%	0%	0%	0%
	2	6%	1%	0%	0%	0%
	3	11%	6%	1%	0%	0%
	4	16%	11%	6%	1%	0%
	5	21%	16%	11%	6%	0%

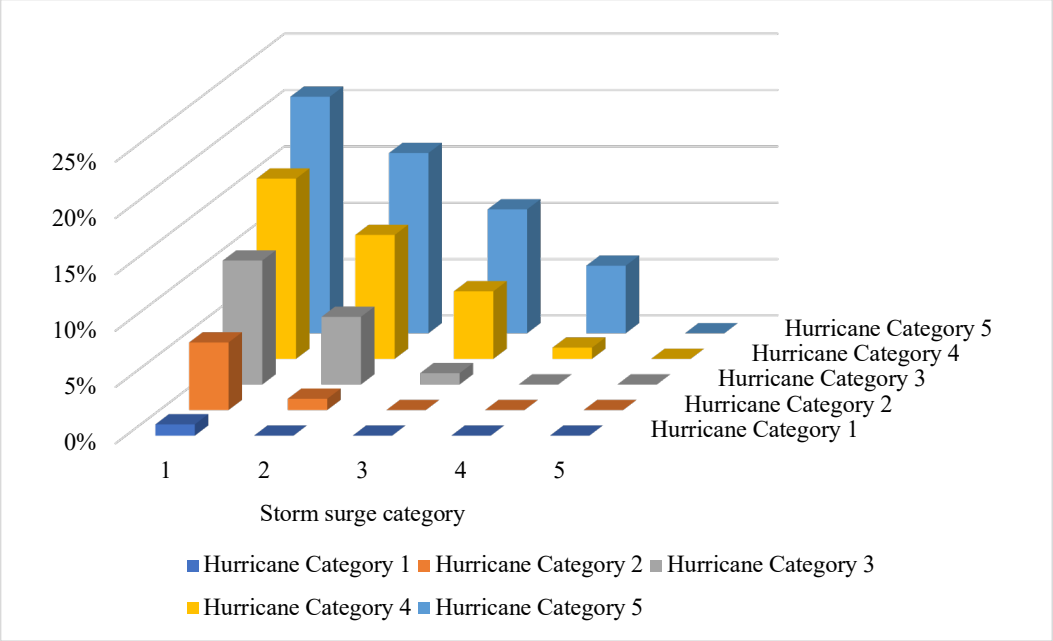

Figure 12. Graphical representation of underground failure rate for data in Table 7

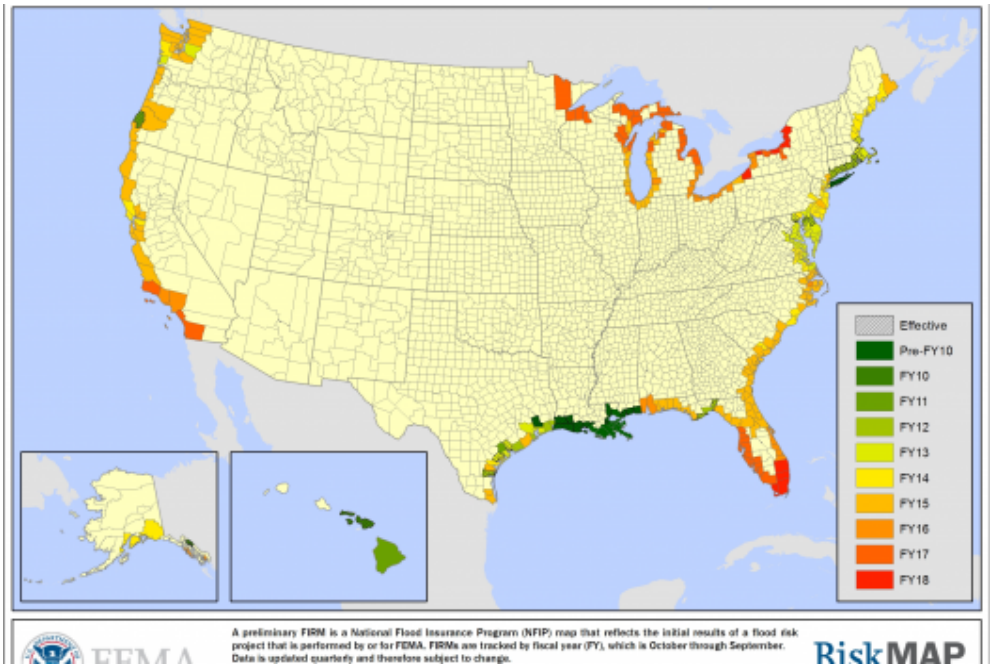

Figure 13. Flood risk map of the United States (FEMA, 2018)

Figure 13 shows the US flood risk map as given by the Federal Emergency Management Agency (FEMA, 2018). It can be seen that most of the coastal areas have high risk of flooding, especially some parts of the north east and Florida.

2.3. Modelling an Earthquake

2.3.1. Introduction

According to USGS (2018), earthquake is "a term used to describe both sudden slip on a fault, and the resulting ground shaking and radiated seismic energy caused by the slip, or by volcanic or magmatic activity, or other sudden stress changes in the earth." When an earthquake of a great intensity occurs, it causes significant loss to human life and property.

An earthquake has three important characteristics as given below. There are mathematical models developed for each of these three characteristics and they are discussed in detail in the following sections.

1. Occurrence
2. Magnitude
3. Intensity /Peak Ground Acceleration

2.3.2. Occurrence of an earthquake

The occurrence of an earthquake in time is governed using Poisson distribution (Vickery et al., 1995). A Poisson distribution is defined by the following equation.

$$f(z) = \frac{e^{-\lambda}\lambda^{z}}{z!} \tag{2.19}$$

Where z is the number of earthquakes per year, λ is the average number of earthquakes that occur in a given year.

We simulate the time between successive earthquake occurrences using exponential inter-arrival time distribution. The equation used to generate a random number with exponential distribution using inverse transform technique is given below and this value represents the earthquake inter-arrival time(t_{eqk}).

$$t_{eqk} = \frac{-\log(1-rand())}{\lambda} \tag{2.20}$$

For example, for a value of λ= 0.5 quakes per year, the simulation results for the annual occurrence is obtained as 0.3430 years which means an earthquake is expected every 0.34 years.

2.3.3. Magnitude of an earthquake

The magnitude of an earthquake is usually measured on a Richter scale with the help of instrument called seismograph. The magnitude scale usually ranges from 2 to 10 and is logarithmic. The Richter scale magnitude can be calculated using the following equation (USGS, 2018).

$$M = log\ A + 2.56 logD - 1.67 \quad (2.21)$$

Where

A=the measured ground motion (in micrometers)

D=the distance from the event (in km).

With this the energy released in Joules can be calculated using the following equation (USGS, 2018).

$$\log_{10} E = 4.8 + 1.5M \quad (2.22)$$

where

E = energy released in the earthquake in Joules.

M= earthquake magnitude in Richter scale.

Table 8. Energy Released for Various Earthquake Magnitudes

Earthquake Magnitude on the Richter Scale	Energy Released (Joules)	Ratio
1	2.0×10^6	N/A
2	6.3×10^7	31.5
3	2.0×10^9	31.7
4	6.3×10^{10}	31.5
5	2.0×10^{12}	31.7
6	6.3×10^{13}	31.5
7	2.0×10^{15}	31.7
8	6.3×10^{16}	31.5
9	2.0×10^{18}	31.7

The British Geological Survey has provided the energy released for various magnitudes are shown in Table 8 below. Note that ratio is defined as the energy released from the current scale versus the energy from its previous adjacent scale. For instance, the energy released in Scale 8 is 31.5 times of the energy released in Scale 7.

2.3.4. Intensity of an earthquake

In order to calculate the extent of damage, there is another scale that is used and known as the Modified Mercalli Intensity scale. This scale ranges from 1 to 12 in the order of increasing levels of intensity. It is based on the observed effects of shaking and does not have a mathematical basis. The description of each level of intensity and the corresponding level of damage is explained in detail in Table 9 (USGS, 2018).

Table 9. Modified Mercalli Intensity Scale (USGS, 2018)

Intensity	Shaking	Description/Damage
I	Not felt	Not felt except by a very few under especially favorable conditions.
II	Weak	Felt only by a few persons at rest, especially on upper floors of buildings.
III	Weak	Felt quite noticeably by people indoors, especially on upper floors of buildings. Standing cars may rock slightly.

Table 9. Continued

Intensity	Shaking	Description/Damage
IV	Light	Felt indoors by many, outdoors by few. Dishes, windows, doors might vibrate, walls make cracking sound. Sensation like heavy truck striking building. Standing cars rocked noticeably.
V	Moderate	Felt by everyone; many awakened. Some dishes and windows might break. Unstable objects overturned. Pendulum clocks may stop.
VI	Strong	Felt by everyone. Some heavy furniture moved; a few instances of fallen plaster. Slight damage.
VII	Very strong	Negligible damage in buildings of good design and construction; considerable damage in poorly built or badly designed structures; some chimneys broken.
VIII	Severe	Slight damage in specially designed structures; considerable damage in ordinary substantial buildings with partial collapse. Great damage in poorly built structures. Chimneys, factory stacks, columns, monuments, walls might collapse.
IX	Violent	Considerable damage in specially designed structures; well-designed frame structures thrown out of plumb. Great damage in substantial buildings, with partial collapse. Buildings shifted off from foundations.

Table 9. Continued

Intensity	Shaking	Description/Damage
X	Extreme	Some well-built wooden structures destroyed; most masonry and frame structures destroyed with foundations. Rails bent.

The intensity of an earthquake is usually expressed in terms of peak ground acceleration (PGA). According to Wikipedia PGA is defined as "The maximum ground acceleration that occurred during earthquake shaking at a location. PGA is equal to the amplitude of the largest absolute acceleration recorded on an accelerogram at a site during a particular earthquake."

An equation for estimating the *PGA* is given below (Espinosa et al., 2017).

$$\ln PGA = 6.36 + 1.76M - 2.73\ ln\ (R + 1.58e^{0.608M}) + 0.00916h \qquad (2.23)$$

where

M=the magnitude of the earthquake on the Richter scale

R=the distance to the epicenter in km

h=the focal depth in km

PGA= peak g round acceleration in gals (cm/s^2).

For example, an earthquake of magnitude M=8, focal depth (h) as 24km will have a peak ground acceleration of 4.5×10^6 cm/s^2 at a distance (R) of 1 km from the epicenter.

2.3.5 Hazard Maps

With the PGA values, hazard maps are usually constructed for an area that provides several details like

- The earthquake history of a particular area to arrive at the probability of an earthquake
- To find the PGA produced by the earthquake in that area
- The geological information, and frequency of shaking, etc.

Figure 14 shows a USGS seismic hazard map for the United States. It shows the frequency of damaging earthquake shaking on the Modified Mercalli Intensity Scale.

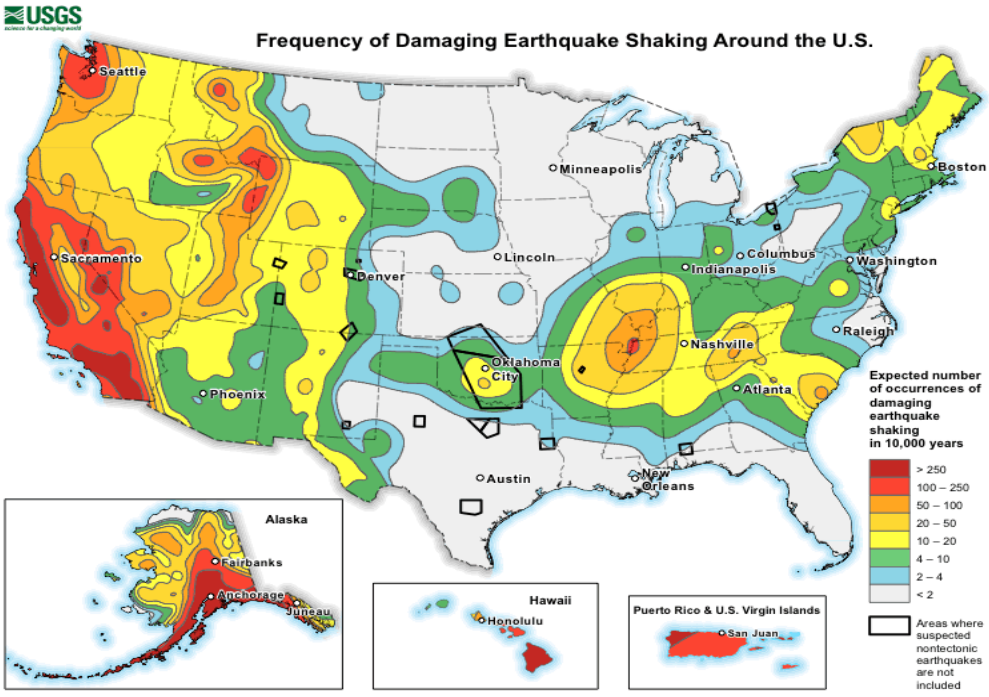

Figure 14. Seismic Hazard Map of the United States (USGS, 2019)

3. REPAIR AND RECOVERY MODEL OF POWER LINES

3.1 Operation of Power Grid System

In the modern digital era, even a small power disruption causes loss of information and reduction in industrial productivity. The cost related to power outages have been increasing steadily. The annual cost of interruption of electricity in the US is around $150 billion a year (Galvin Power, 2019). The following table shows the losses incurred in various business sectors for a one-hour power interruption.

Table 10. Average cost of one-hour power disruption in the US (GalvinPower, 2019)

Industry Sector	Average cost of one-hour interruption
Cellular communication	$ 41,000
Telephone ticket sales	$ 72,000
Airline reservation system	$ 90,000
Semiconductor manufacturing	$ 2,000,000
Credit card operations	$ 2,580,000
Brokerage operations	$ 6,480,000

In spite of several protection measures, owing to the complexity and size of the power system network outages happen due to several reasons like human error, technological glitches, criminal and terrorist activities, extreme weather events or other natural disasters. Hurricanes represent a significant portion of all the extreme weather events that took place in 2017 and 2018. They not only affect the economic activities of day to day life, but also pose a great threat to the power system operations. Even though an extreme weather event

can be predicted, and necessary precaution be taken, it can only reduce the damage incurred to some extent.

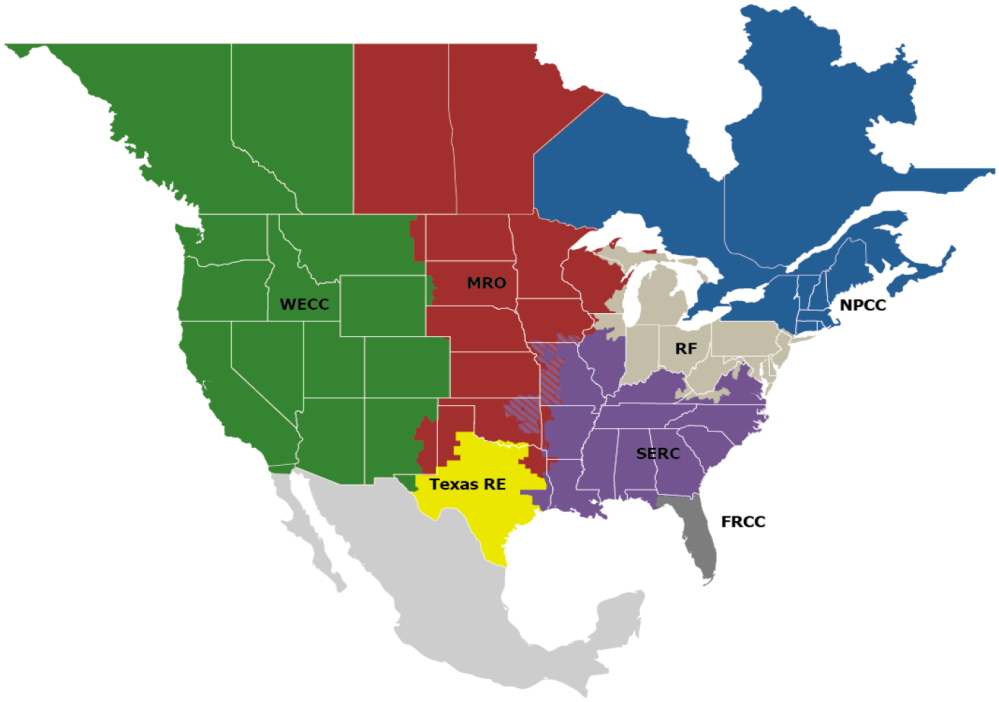

Figure 15. North American Bulk Power System (NERC,2018)

Figure 15 above shows the North American bulk power system. It can be seen that there are seven regional entities that power various areas of the US. Among these, the states of Florida and Texas have stand-alone grids. This makes it all the more necessary for these two power grids to be more resilient as Texas and Florida face flooding and hurricane very frequently.

Figure 16 shows the hierarchical structure of a typical power grid with its components. It mainly consists of three types of units: the generating unit, the transmission unit, and the distribution unit. The generating unit is where the electric power is produced. It could be thermal power plant, nuclear plant, hydroelectric, solar, wind or any other form of power sources. The power produced is escalated to a high voltage level using step-up

transformers so that it can be transferred over long distances with less energy loss. The receiving end consists of step-down transformers which bring the high voltage down to a low level that is suitable for use by commercial, industrial and residential customers. In the end, the distribution lines stemming from the step-down transformer deliver the power to the end user. Apart from the main generating station, the modern grid also consists of several active distribution resources connected to the grid like the roof-top solar panels, onsite wind turbines and electric vehicles fleet. The end customers not only take power from the main grid but also return surplus power to the grid and are generally termed as "prosumers" under the transactive energy marketing mechanism. The power flow in a modern grid is in two ways as can be seen in Figure 16.

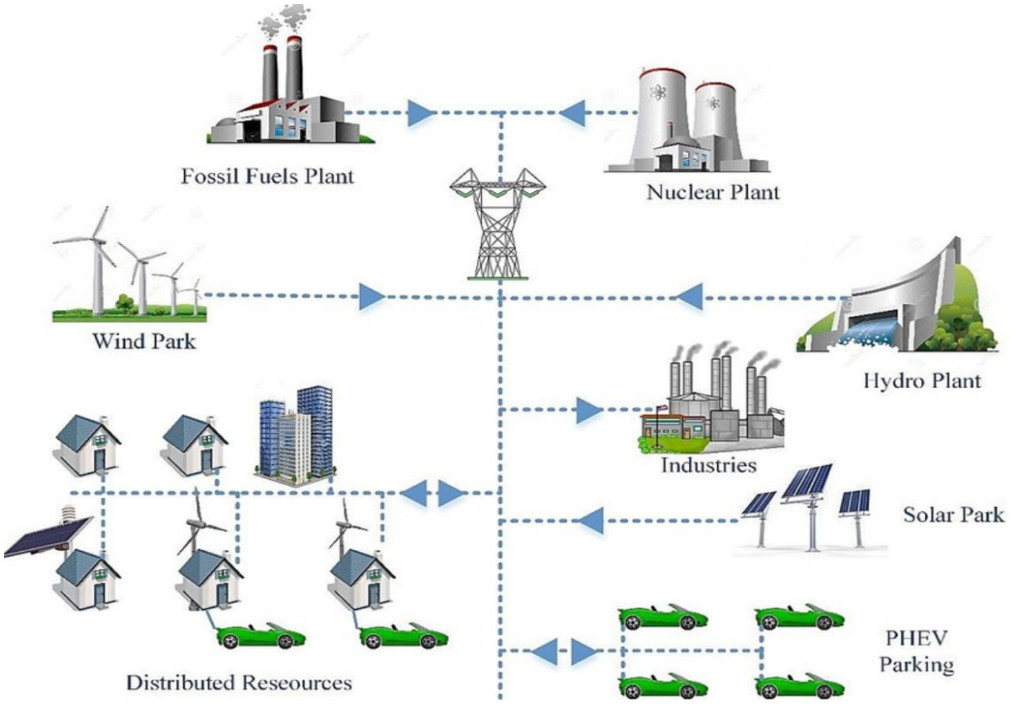

Figure 16. Typical power grid system (Modern Power grid, 2019)

3.2 Power System Components

Extreme event analysis report by several public organizations such as Electric Reliability Council of Texas (ERCOT), Board of Public Utilities (BPU), North American Electric

Reliability Council (NERC) state that most of the power outages following a disaster event occurs mainly due to the failure of outdoor grid components like transmission and distribution lines, step-up and step-down transformers, and generators. Even though burying power lines underground might be considered as a potential alternative, it is not a cost-effective approach in reality. The cost to convert an overhead line to underground might be around $80,000 per mile in rural areas and $2 million per mile in an urban area (BPU, 2012). Post a disaster, the recovery should be done in a swift manner to restore power outages. Recovery involves sending the repair crew to the affected areas and replacing or repairing the damaged components of the power grid.

There are several challenges during the recovery process. For example, once the event has taken place, customers should have an idea of estimated time to restoration so that commercial and industrial customers can plan ahead. The recovery of a power system is delayed or becomes difficult due to several factors, such as coping up with extreme weather conditions, difficulty in communicating among the transmission system operators (TSO), issues in accessing to the affected area, and lack of availability of trained personnel and rapid mobilization. In fact, the accessibility issue is largely due to flooding or roadblocks by fallen trees and distribution lines.

3.3. The Recovery Model of Transmission and Distribution Lines

Literature review shows that the repair and restoration of power lines can be analyzed using Markov chain model (Jin et al., 2018). The following figure shows the transition diagram for restoration of transmission/distribution lines. Let K be the total number of lines that are susceptible to failure under extreme weather. The failure time and the repair time of a line are exponentially distributed with rate λ and μ, respectively. Here failure rate refers to the

number of power lines failing per unit time and repair rate refers to the number of lines repaired or recovered per unit time. Let R be the total number of repair teams available to undertake the recovery process.

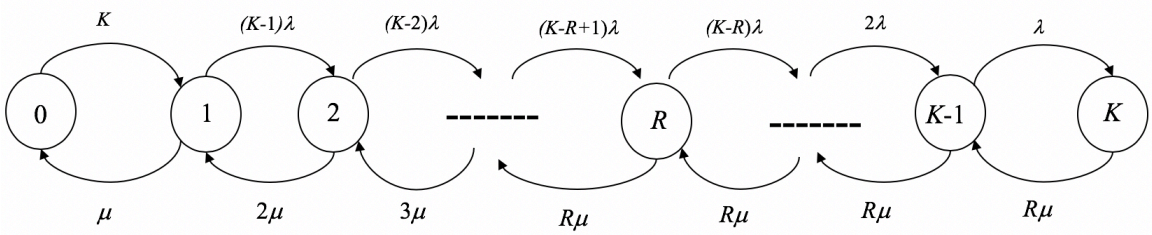

Figure 17. Markov Transition diagram for recovery of power lines.

Table 11. Table of Notation for repair and recovery model of transmission lines

Symbol	Description	Units
K	Total number of power lines subject to failure	Line
λ	Failure rate	Lines/hour
μ	Repair rate	Lines/hour
R	Number of repair teams	Team
L	Expected number of failed lines	Line
L_q	Average number of failed lines in waiting for repair	Line
L_s	Average number of failed lines under repair	Line
W	Expected recovery time of a line	Hour
W_q	Average waiting time of a failed line for repair	Hour
W_s	Average service time of a failed line	Hour

The steady-state probability of the system π_k is given by the following equation.

$$\pi_k = c_k \pi_o, \quad \text{for } k=1, 2, 3, \ldots, K \tag{3.3}$$

The values of c_k and π_o in Equation (3.3) are calculated using the following formulae.

$$c_k = c_{k-1} \frac{\lambda_{k-1}}{\mu_k} \tag{3.4}$$

$$\pi_o = \frac{1}{1+\sum_{k=1}^{K} c_k} \quad \text{for } k=0 \tag{3.5}$$

Performance indices such as expected number of damaged lines (L), expected recovery time(W), average waiting time before recovery (W_q), average number of failed lines waiting to be repaired (L_q) can be calculated using Little's law as given below.

$$L = \sum_{k=0}^{K} k\pi_k \tag{3.6}$$

$$L_q = \sum_{k=R}^{K} (k-R)\pi_k \tag{3.7}$$

The number of lines under service (L_s) is given by the following equation.

$$L_s = L - L_q \tag{3.8}$$

The expected recovery time (W) is given by the following formulae.

$$W = \frac{L}{\sum_{k=0}^{K} (K-k)\lambda\pi_k} \tag{3.9}$$

3.4. Application to Hurricane Harvey

Hurricane Harvey is a Category 4 hurricane that made a landfall in Rockport, Texas on August 25, 2017. Figure 18 shows Harvey's landfall site and its moving track on land. After its landfall, it moved in land for a total of five days from August 25 to 29. It can be seen that eventually Harvey became a tropical storm and faded away after nine days. Harvey caused both flooding and major physical damage to the bulk power system in Texas, Louisiana, Tennessee and Kentucky. There were two million customer outages reported after the hurricane landfall (NERC, 2019). Major damage to the transmission system was caused by hurricanes and tornadoes in the areas of Victoria, Port Aransas to

Corpus Christi. In addition, Houston, Galveston, Beaumont, Port Arthur were affected by flooding. Some of the transmission system damages include the following.

- Static wire and conductor damages.
- Broken poles and insulators.
- Damage from trees being blown away by strong wind.
- Flooded substations and control houses.

During the hurricane onslaught, the assessments on damage also became difficult and were delayed due to several challenges faced and some of them are mentioned below (NERC, 2019).

- Heavy debris on roads.
- Wind damages to substation and control house roofs and windows.
- Flooding in relay systems, transmission tower foundations damage due to flooding.
- Inability to use trucks due to strong winds.

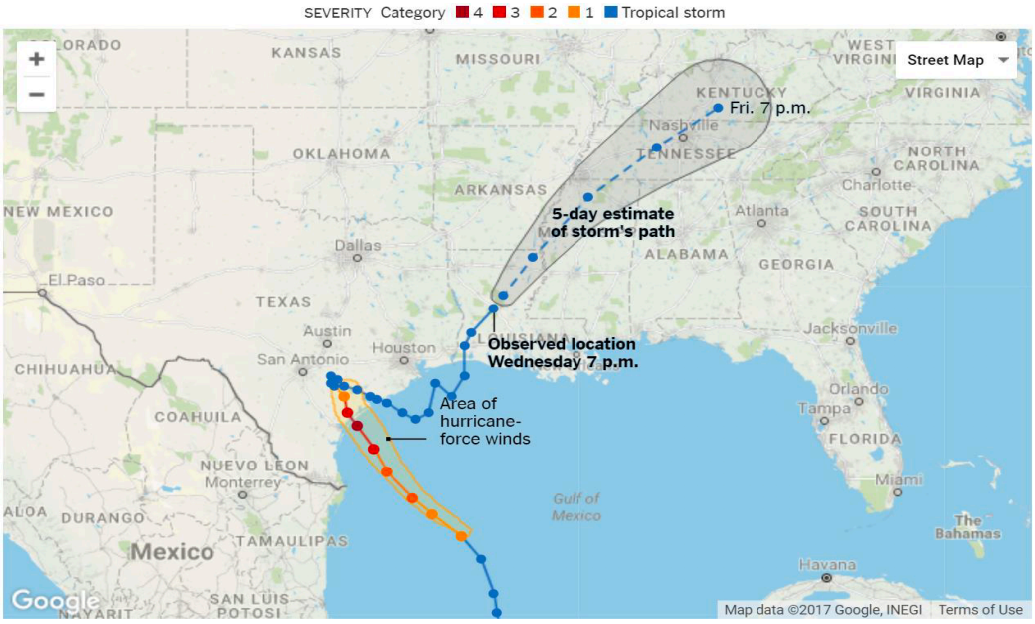

Figure 18. Hurricane Harvey's track (ERCOT, 2018)

Figure 19. Damaged distribution line

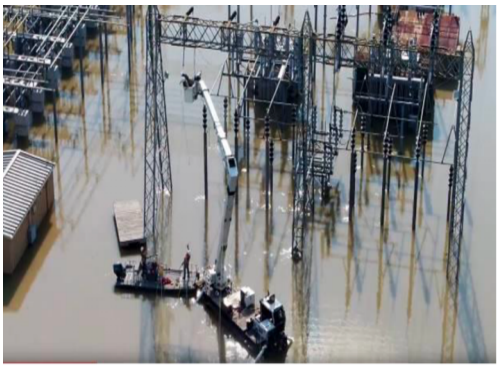

Figure 20. Flooded Substation

Figure 21. 345KV line structures down

Figure 22. Recovery operations post Harvey

Figure 23. Broken wooden pole

Figure 24. Recovery post floods from Harvey

The above figures show the aftermath effect of Harvey as released by NERC Event Analysis report.

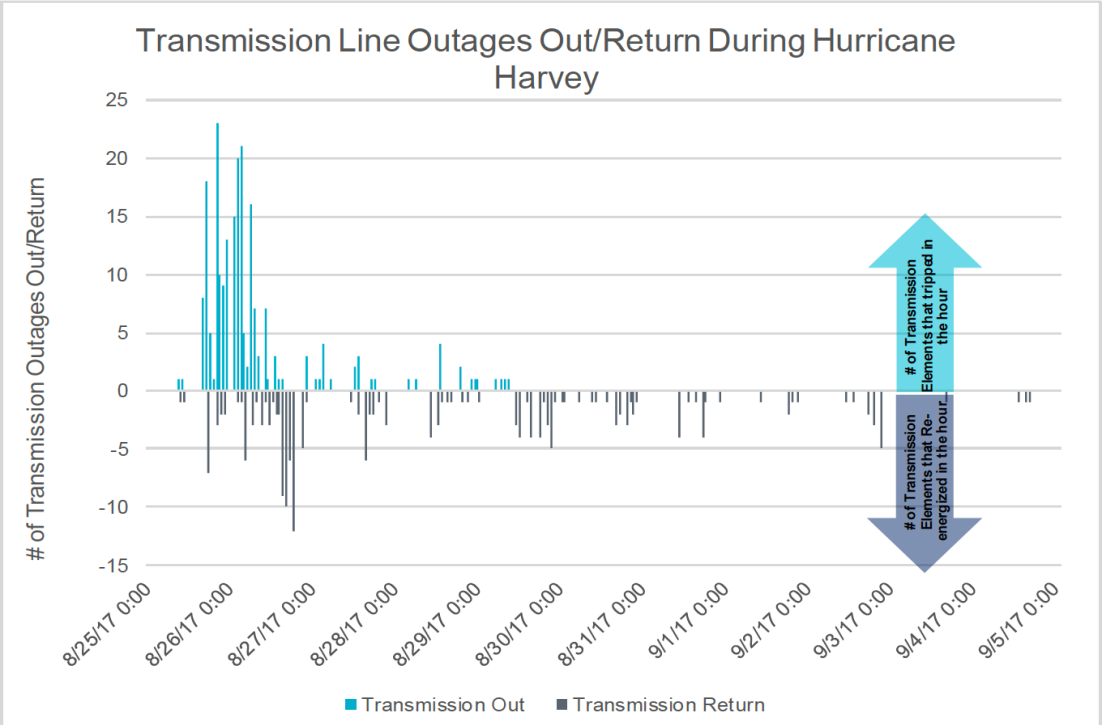

Figure 25. Hurricane Harvey transmission line outage/return data (ERCOT, 2018)

The extreme event analysis report of ERCOT for hurricane Harvey provides transmission lines outages and recovery data as shown in Figure 25. Using this data set, we can know the number of lines that failed and were restored every day which is tabulated in Tables 12 and 13, respectively.

Table 12. Transmission line outage data for Hurricane Harvey

Day of Event (MM/DD/YY)	Number of Line Damaged
8/25/17	2
8/26/17	184
8/27/17	10
8/28/17	9
8/29/17	14

Table 13. Transmission line recovery data for Hurricane Harvey

Day of Event (MM/DD/YY)	Number of Lines Restored
8/25/17	2
8/26/17	47
8/27/17	35
8/28/17	24
8/29/17	22
8/30/17	16
8/31/17	18
09/01/17	31
09/02/17	6
09/03/17	10

It can be seen that on August 26, 2017 the failures reached the maximum. This is because the hurricane made a landfall at peak intensity on August 25 at 10:00pm and then it slowly moved inland. Since the exact time of failure of each transmission line is not shown in Figure 24, we generate the failure time of each line using uniform random distribution between 0 and 24 hours and used it to calculate the inter arrival time between subsequent failures. This was again repeated for calculating the repair rate across a day. Then this inter-arrival time was used to calculate the failure rate and repair rate using the following equations.

λ= (Total number of failed lines)/(Sum of the inter-arrival times) (3.8)

μ= (Total number of recovered lines)/ (Sum of the inter-arrival time) (3.9)

We obtained a failure rate of 1.84 lines per hour and recovery rate of 0.82 lines per hour. This value was verified again by calculating the failure rate and recovery rate directly from

the given data in Figure 24 without randomly generating the inter arrival time in a given date.

3.5. Sensitivity Analysis and Results

The Markov chain model was implemented in MATLAB and the performance metrics is computed for various values of lines K, repair teams R, failure rate λ and recovery rate μ. The results are discussed in detail in the following section. Serving as the benchmark, we take λ=1.84 lines per hour, μ=0.82 lines per hour, R=30, and K=200 as the baseline for evaluating various performance metrics.

3.5.1. Effect of repair rate on L, W and W_q

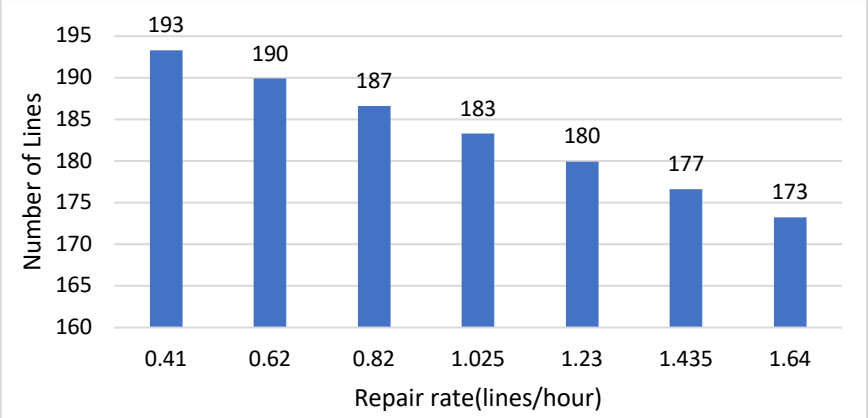

Figure 26. Repair rate versus expected no. of failed lines (L)

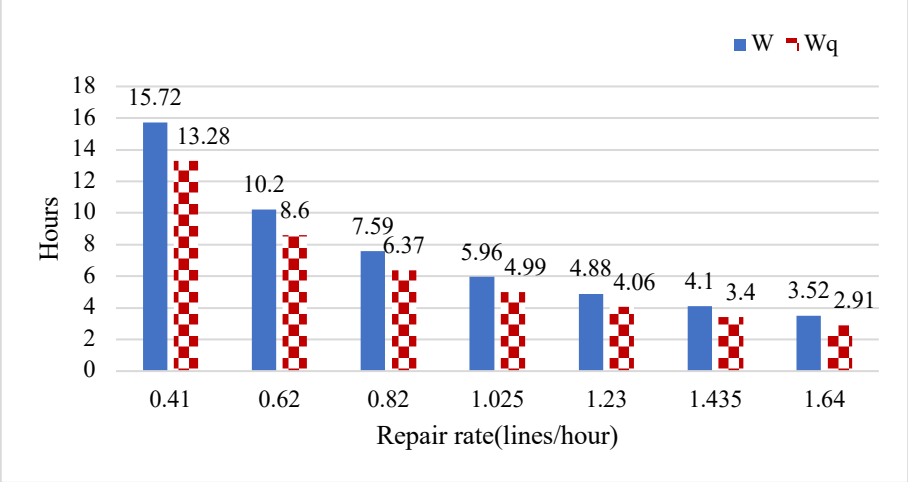

Figure 27. Repair rate versus expected recovery time (W)

For a given value of K and failure rate (λ), it can be seen that as the repair rate increases, the values of L, W, W_q decreases. If the repair rate is doubled from 0.82 lines per hour to 1.64 lines per hour, L reduces by 7.7% whereas W reduces by 53%. If the repair rate is halved to 0.41 lines per hour, L increases by 3.5 % whereas W increases by 107 %. It can be seen that W_q also increases accordingly in Figure 26. Repair rate gets affected when the recovery procedures are hampered due to flooding, heavy debris lying on roads etc. From Figure 27 we can see that reduction in repair rate affects W to a great extent which means customer outages will be prolonged.

3.5.2. Effect of failure rate on *L* and *W*

It can be seen from Figure 28 that as the weather severity increases which eventually leads to an increased failure rate, L and W also increase. If the failure rate increases by 50%, L and W increase by 2.37 and 2.38%, respectively. If we double the failure rate as it might happen in the case of a Category 5 hurricane, L increases by 3.58% and W increases by 3.95%. For hurricanes of lower category, where the failure rate might be 50% lesser, it could be seen that L decreases by 7.1% and W decreases by 7.7%.

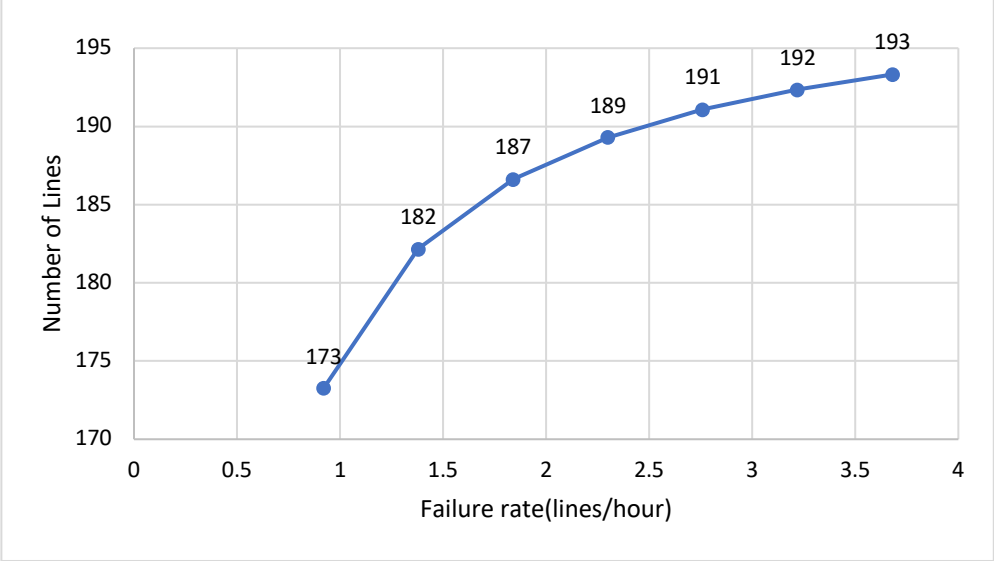

Figure 28. L versus failure rate

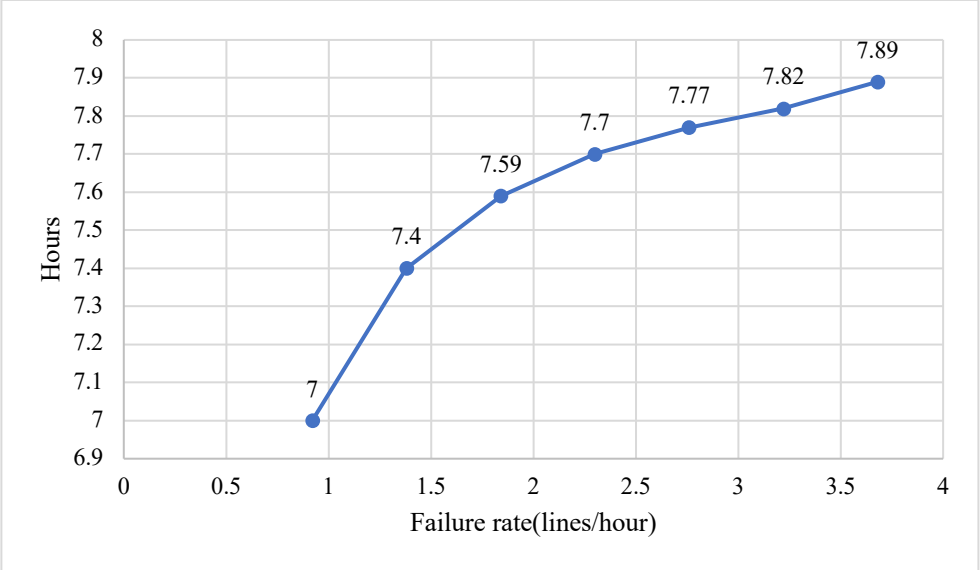

Figure 29. W versus failure rate

3.5.3. Effect of number of repair teams on L, L_q, W and W_q

We now analyze how the number of repair teams R participating in the recovery process affect the value of L and W. For this case, we keep the repair rate constant. If R is doubled from 30 to 60, it can be seen that L reduces by 7.7% which is the same as that of doubling the repair rate. This shows that doubling the repair rate or the repair crew both have the same effect on the system recovery speed. The same holds true if we reduce the number of repair teams. The same can also be observed for W as well.

The recovery time and average waiting time in queue for failed lines also change in the same manner with respect to the change in repair teams as they do with repair rate. However, along with increasing the number of repair teams there are few alternative measures that can be taken in order to speed up the damage assessment phase after an extreme event such as:

- Using high water boats to access flooded areas.

- Using aerial drones to survey and perform damage assessment where roads are blocked by debris.

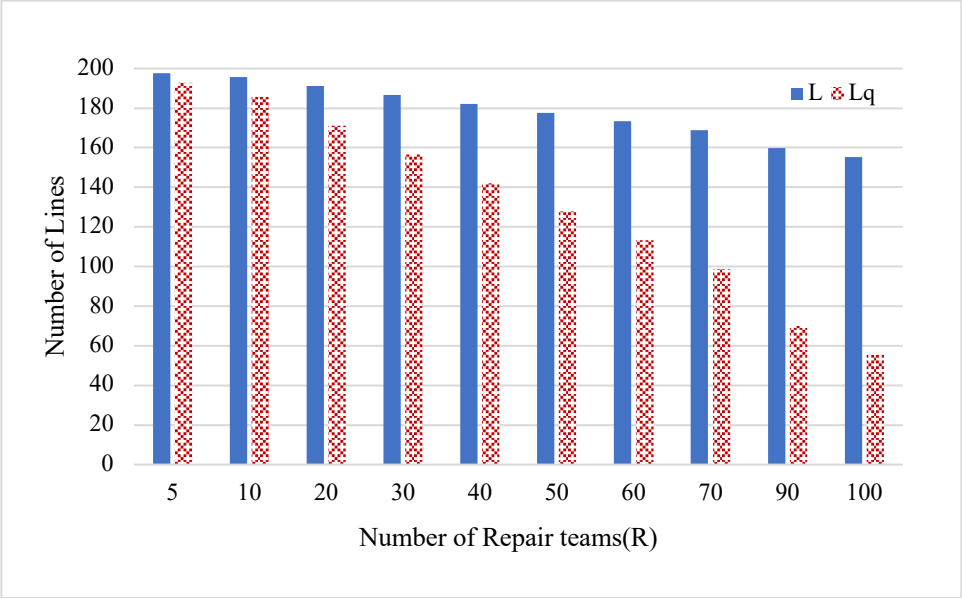

Figure 30. *L, L_q* versus repair rate

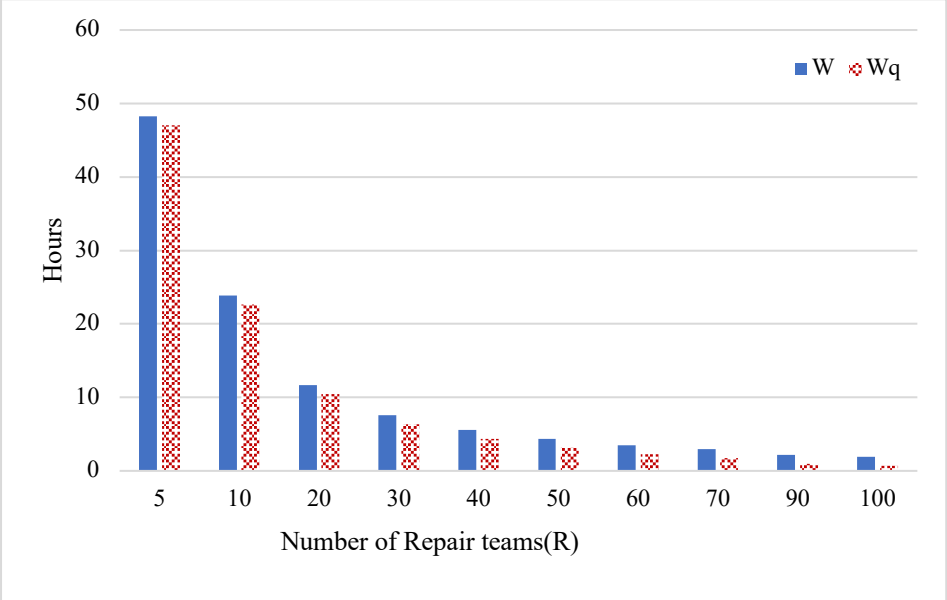

Figure 31. *W*, W_q versus repair teams

3.5.4. Effect of *K* on number of repair teams

For a given value of recovery rate, if the number of transmission lines increase, the repair teams needs to be increased accordingly to maintain the restoration time. If this does not

happen then it might lead to longer restoration times in the aftermath of an event. This becomes particularly significant in those cases where the damage severity is far more than anticipated. Several hurricane event analysis reports state that hurricanes like Irma and Harvey caused more damage than anticipated because they are intensified into a powerful category before they made a landfall. In such cases increasing the repair crew would be the only option as the repair rate cannot be further improved. This is mainly because performing recovery operations will be hampered by the harsh weather conditions and catastrophic damages.

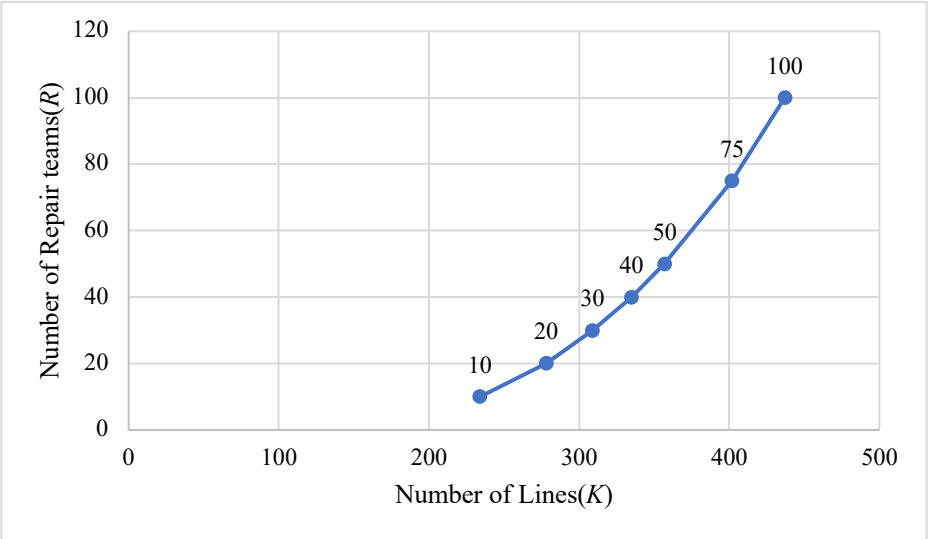

Figure 32. *K* versus repair teams

In summary, we can say that more the weather severity is, the more damage to the power system and increased customer outages. To tackle the situation two different solutions are possible: either increasing the repair rate or increasing the number of repair teams as both have the same effect on the system. This is also important because the power grid needs to serve the critical loads during the extreme weather as well as in the aftermath of the event.

4. ELECTRIC VEHICLES FOR ATTAINING GRID RESILIENCE

Man-made and natural events cause power interruptions and prevents the electrical grid from providing reliable, high quality power. This causes heavy losses to producers and consumers as they are becoming increasingly dependent on reliable power supply to compete globally. This situation raises the need to identify cost effective strategies that can improve the power grid resilience. The increase use of electrical vehicles (EVs) could serve as a good alternative to improve the grid resilience. The energy available from an EV can be used in three different ways to enhance grid resilience, namely Grid -To-Vehicle (G2V), Vehicle-To-Building (V2B) and Vehicle-To-Grid (V2G). The following sections of this chapter discuss in detail about modeling of an EV battery swap process and the calculation of power available from an EV.

4.1. Battery swap station

A typical electric vehicle (EV) battery swap station consists of fully charged spare batteries readily available. When an EV arrives at the station, the empty battery is removed from the vehicle. The already charged spare battery is put into the vehicle and the vehicle leaves the charging station. The depleted battery is left in the station for recharging. When it gets fully charged, the battery is moved to the inventory for future swapping. Depending upon the battery capacity of the EV, the charging time may vary. For instance, for the first-generation Nissan Leaf, it usually takes 2-3 hours for fully recharge the 24kWh battery using Level 2 charger, yet it only needs 30 minutes if Level 3 charger is used.

4.2 Modeling an Electric Vehicle battery swap process

The service of a battery swap station can be modeled using queueing theory. Let s be the number of spare batteries available at a station, and λ be the rate of arrival of the EV into the swap station. Further let μ be the charging rate of the charge points for recharging the depleted battery in the station. The following transition diagram describes the various states for this swap process.

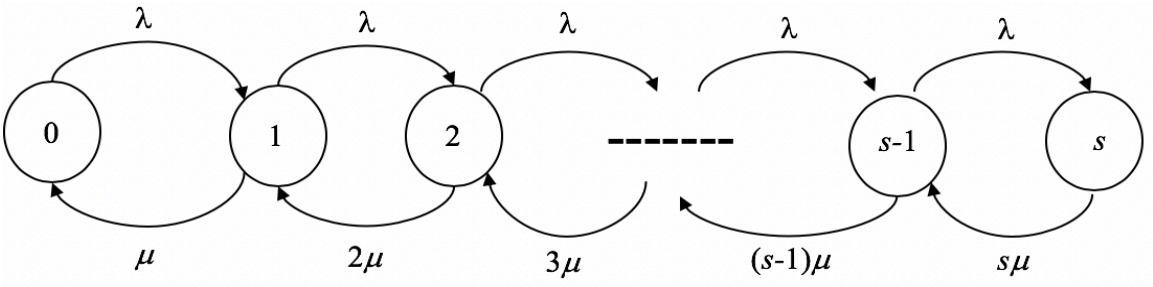

Figure 33. Birth - death process of an Erlang B queuing system.

The queueing model in Figure 33 is also known as Erlang B queue. Here state '0' signifies that there is no empty battery in the station, meaning there are s fully charged battery packs available in the stock. On the other hand, state 's' signifies that there are no spare batteries available, meaning all battery packs in the station is under recharging. When an incoming vehicle finds out that there are no spare batteries available, it has to leave the swap station and find alternative approach to recharge the battery. For instance, the EV has to choose to charge the onboard battery directly using supercharger. For Erlang B model, the system has a finite capacity 's' and there are no waiting positions for battery swapping. This behavior of an Erlang B system is expressed as $M/G/s/s$ in the Kendall's notation. Here M represents Markovian arrival process and G represents the general service time, and 's' represents the number of servers in the system. In our case, it is the number of spare batteries in a station. The queue discipline is first-come-first-

served (FCFS) basis. Since there are '*s*' servers in the system, the maximum service rate is $s\mu$ where μ is the recharge rate of an individual battery. The steady state probability of state '0' is given by the following equation (Privault, 2013)

$$\pi_0 = \frac{1}{1+\sum_{j=1}^{s} c_j} \quad \text{for } j=1, 2,\ldots\ldots s. \tag{4.1}$$

where

$$c_j = \frac{1}{j!}\rho^j \quad \text{for } j=1,2,\ldots.s. \tag{4.2}$$

The term ρ is defined as the traffic intensity and is given by

$$\rho = \frac{\lambda}{\mu} \tag{4.3}$$

The steady state probability for the different states is given by

$$\pi_j = c_j \pi_0, \quad \text{for } j=1, 2, \ldots, s. \tag{4.4}$$

The steady state probability corresponding to state 's' is denoted as π_s and is given by the following equation.

$$\pi_s = c_s \pi_0, \tag{4.5}$$

where π_s denotes the probability that the system is full (in our case there are no more spare batteries available for the incoming EV). Therefore, π_s also represents the probability of being blocked. Since there are no waiting positions available in the system, the number of waiting EV, $L_q=0$, and the customer waiting time, $W_q=0$. Therefore, the number of EV under service is $L_s=L$, and the total service time is $W_s=W$.

4.3. Optimizing the number of spare batteries for various EV models

There are several EV models available in the market like Nissan Leaf, Tesla and Volt, etc. The use of EVs is also on the rise for the past decade as they help reduce the consumption of fossil fuels and mitigate the environmental impact. The charging stations technology is regulated by SAEJ1172 which is a North American Standard by the Society of Automotive engineers (SAE, 2018). It consists of three levels of charging depending on the voltage, current and power. Table14 shows the respective electrical rating of these levels.

Table 14. Charging Topologies (SAE, 2018)

Level	Description	Voltage and Current	Power (KW)	Approx. time to charge
1	Residential	110V,15A	1.4	18 hours
2	Residential/Public	220V,15-30A	3.3	4-8 hours
3	Commercial	480V,167A	50-70	20-50 minutes

It can be seen that Level 1 is mainly used for residential purposes whereas Levels 2 and 3 are used for public and commercial services. Apart from these there are Tesla superchargers available which are used to charge Tesla car batteries. The supercharger has a power of 120 KW and has an approximate charge time of 75 minutes for Tesla Model S with a battery size of 100 kWh (Tesla, 2019).

Table 15. Tesla Supercharger Technology

Level	Description	Power (KW)	Approx. time to charge
4	Supercharger Technology I	120	75 minutes
5	Supercharger Technology II	350	Data not available yet

For our study, we consider various battery-powered electric cars with a broad range of battery capacity. Table 16 lists the chosen EV for which the battery capacity varies from 24kWh to 100kWh representing today's typical EV models in the market. Though certain cars like Tesla come with a range of different battery capacities for the same model, we choose those capacities that would help in analyzing a broad range of applications.

Table 16. Battery capacity of various EVs in the market

Electric Vehicle	Battery Capacity (kWh)
Nissan Leaf First Generation	24
Nissan Leaf Second Generation	40
Tesla 3	50
Tesla X	75
Tesla S	100

Our next step is to find the charging rate for each of these cars for various levels of charging and the supercharger. The charging time in each case can be estimated using the formula

$$t = \frac{c}{p} \tag{4.6}$$

where

t is the charging time of the battery.

c is the battery capacity of the car in kWh.

p is the charging level power in kW.

The charging rate is given by following equation,

$$r = \frac{1}{t} \tag{4.7}$$

where r is the charging rate corresponding to different levels of charging technologies. The charging rate for each case is listed in Table 17. This represents the service rate (μ) of Erlang B queue. Since Level 1 is used only for residential purposes, we calculate the charging time based on Levels 2 and 3, and the superchargers (Level 4 in Table 15).

Table 17. Charging rate of EVs wrt. various charging levels.

Electrical Vehicle	**Level 2 (car/hour)**	**Level 3 (car/hour)**	**Tesla Supercharger (car/hour)**
Nissan Leaf First Gen.	0.1375	2.083	5
Nissan Leaf Second Gen.	0.0825	1.25	3
Tesla S	0.033	0.5	1.2
Tesla X	0.055	0.66	2
Tesla 3	0.066	1	2.4

We assume various EV arrival rate like λ =1, 3, and 5 cars/hour and optimize the number of spare batteries required for different blocking probability, namely π_s=1%, 5%, and 10%.

4.4. Results and Discussion

We analyze how the number of required spare battery varies for different EV arrival rate at different charging levels. The detailed results are presented in Figures 34-36.

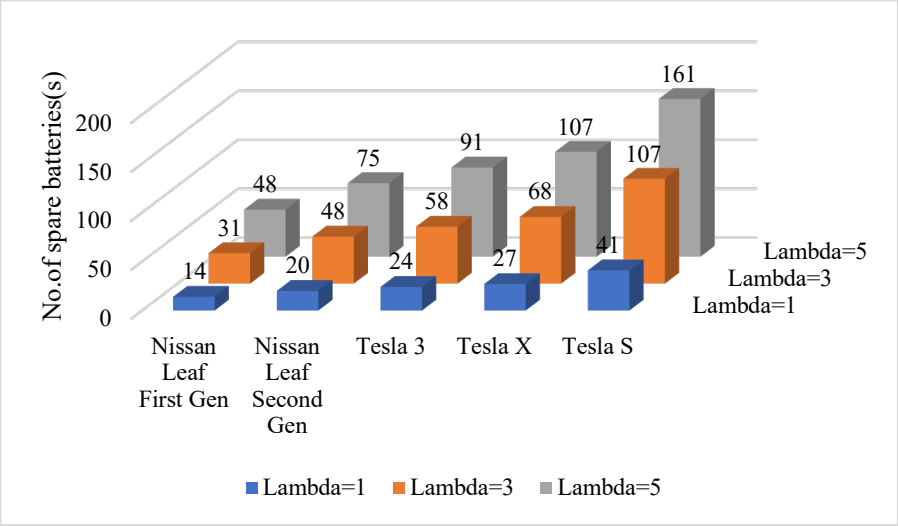

Figure 34. The Minimum *s* under Level 2 charging with 1% blocking probability

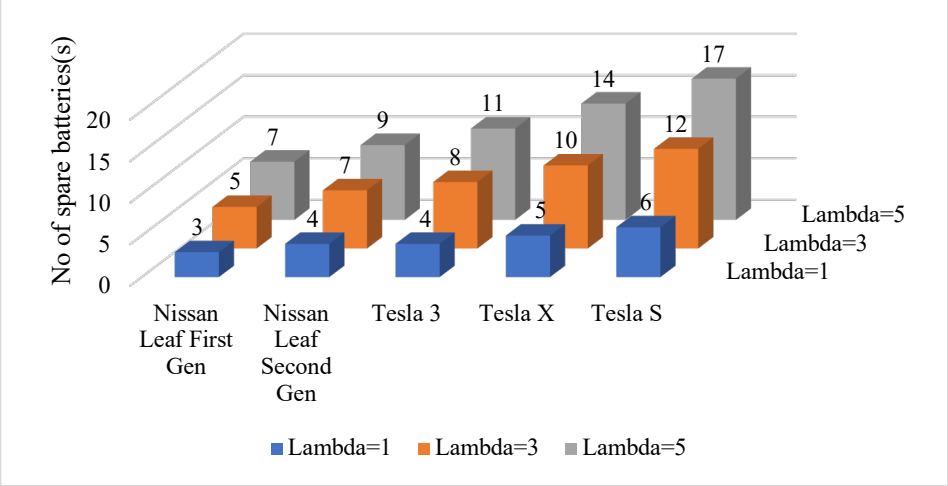

Figure 35. The minimum *s* for Level 3 charging for 1% blocking probability

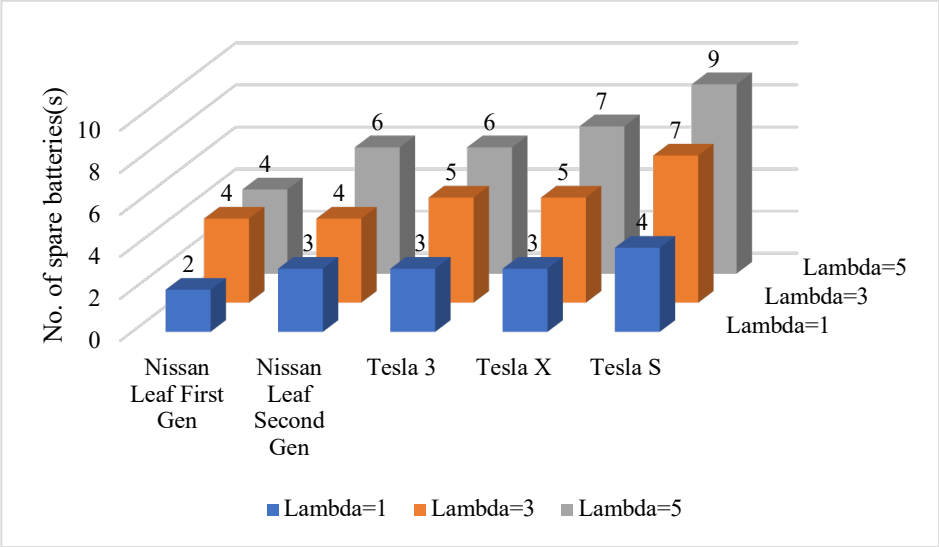

Figure 36. The minimum *s* for supercharger for 1% blocking probability

As expected, when we move towards higher level of charging, the number of spare batteries get reduced. Among all the levels, superchargers require the least amount of spare battery stock due to the shortest charge time. Also, since Tesla S has the largest battery capacity of 100 kWh, it requires more spare batteries compared to any other EV in all the cases. For Level 2 charging the spare batteries range from 14 to 161 for different blocking probability. For level 3 charging, the range decreases to 3-17. Finally, when we use superchargers, the requirement drops down considerably to 2-9. An interesting observation is that as the number of EV arriving to the battery swap station increases, the spare battery requirement does not increase proportionally. For instance, we can observe from Figure 34 that when the EV (Nissan Leaf Second Generation) arrival rate increases from 1 to 5, the minimum number of required spare batteries increases from 4 to 9.

Table 18 shows for a given EV arrival rate, how the spare battery requirement varies with different blocking probability. Here Nissan Leaf I denotes the first generation model and Nissan Leaf II denotes the second generation model.

Table 18. Probability of blocking for various levels of charging

EV Models	Probability of Blocking (π_s) for λ =5 cars/hour								
	Level 2			Level 3			Tesla Supercharger		
	1%	5%	10%	1%	5%	10%	1%	5%	10%
Nissan Leaf I	48	42	38	7	5	3	4	3	3
Nissan Leaf II	75	66	60	9	7	6	6	5	4
Tesla S	161	153	143	17	14	12	9	8	6
Tesla X	107	95	88	14	12	10	7	6	5
Tesla 3	91	81	74	11	9	8	6	5	4

The above table is represented in graph in Figures 37-39 below where PB stands for probability of blocking.

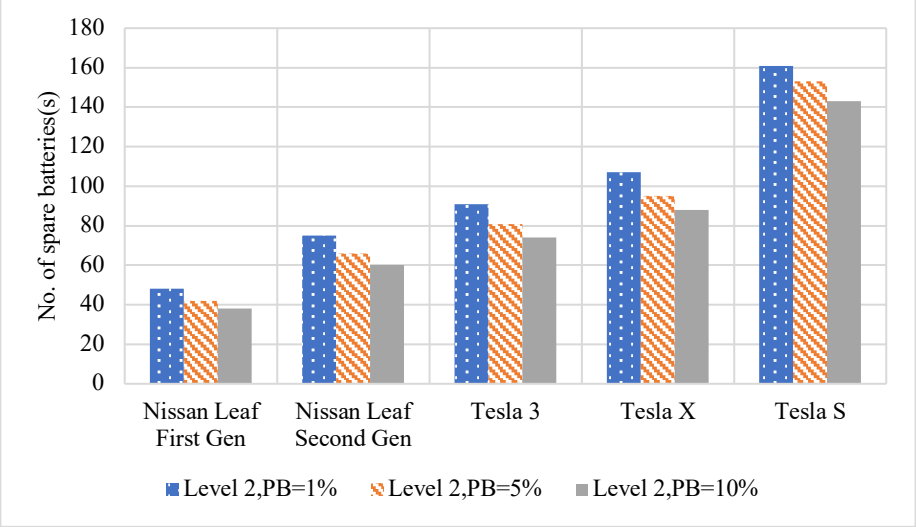

Figure 37. Spare battery requirement for Level 2 charging

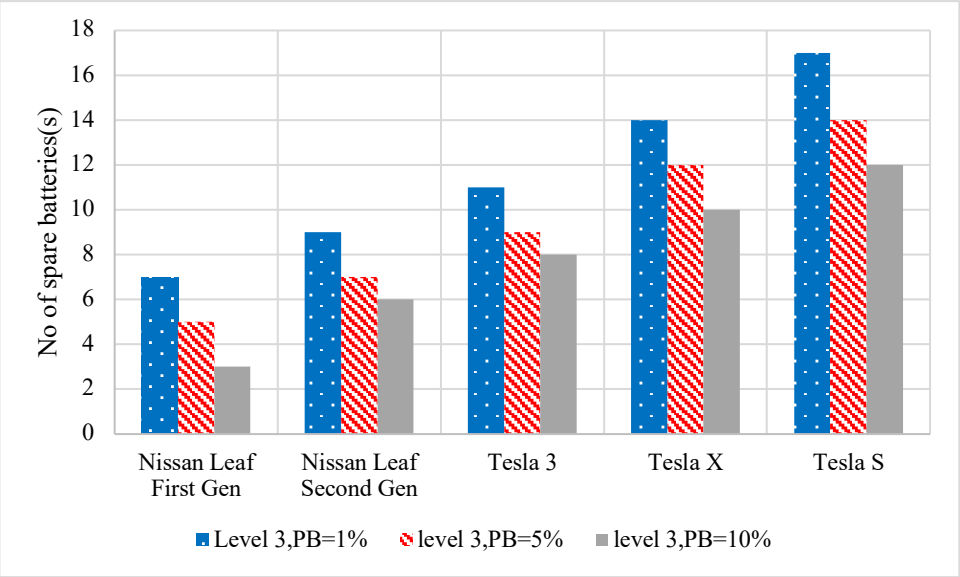

Figure 38. Spare battery requirement for Level 3 charging

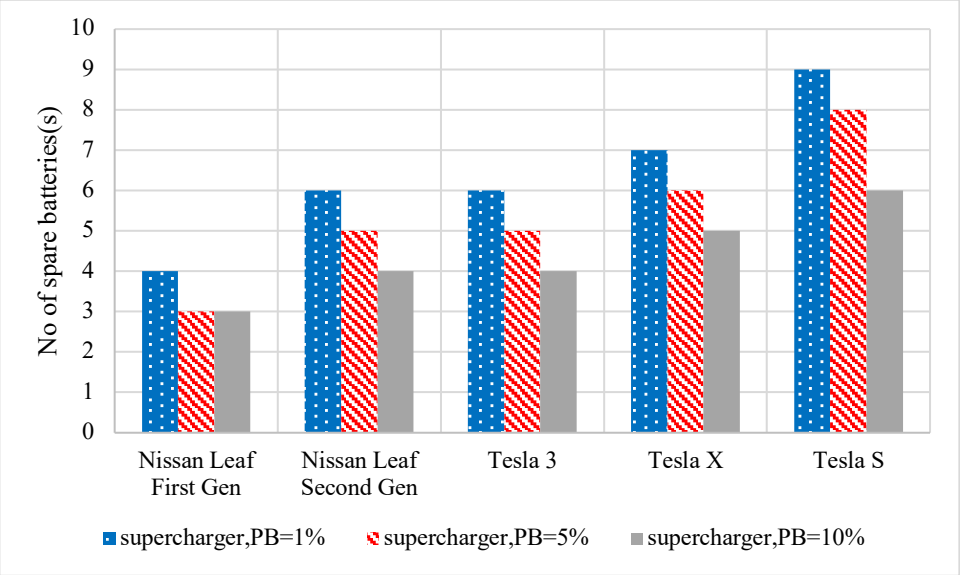

Figure 39. Spare battery requirement for supercharger

4.5 Calculating the Energy and Power Available from an EV

In this section we analyze how a fleet of EV can be used to support the operations of a manufacturing facility or warehouse in case of emergency in the aftermath of an extreme weather event. The first step is to calculate the duration of availability of the EV for

energy use. In case of a BEV, energy can be provided only from the battery of the vehicle whereas in a HEV energy can be provided from the gasoline as well as the battery.

For an HEV the energy available from the gasoline is represented as E_g and is given by the following expression (Rahimi et al., 2017).

$$E_g = \eta_{tank} \times cap_{tank} \times 34 \tag{4.8}$$

where

η_{tank} =the thermal efficiency of the HEV.

cap_{tank} =the capacity of the gasoline tank in gallons and

Note that 34 kWh is the energy produced by burning one gallon of gasoline. The energy from the battery is represented as E_b and is given by

$$E_b = (\text{Maximum discharge}) \times cap_{battery} \tag{4.9}$$

where Maximum discharge is the maximum allowable discharge limit for the battery and $cap_{battery}$ is the battery capacity of the EV.

Finally, the energy stored in the battery and the energy from the gasoline should be converted into alternating current (AC) energy so that it can be used by the manufacturing facility. If the inverter efficiency is denoted as $\eta_{inverter,}$ the total available AC energy (E_{AC}) is given by expression 4.10.

$$E_{AC} = \eta_{inverter} \times (E_b + E_g) \tag{4.10}$$

For a BEV, the term E_g in the above expression is zero because there is no gasoline use. Table 19 shows tank capacity, battery capacity and the energy available to the AC loads in a full tank scenario. In the following table, Prius and Camry Hybrid have a thermal efficiency of 40% whereas Chevy Volt has a thermal efficiency of 37%.

Table 19. Energy Available to AC Loads for various car models (Rahimi et al., 2017)

Vehicle Model	Tank		Battery		Available DC Energy (kWh)	Available AC Energy (kWh)
	Capacity (gallon)	Equivalent in kWh	Capacity (kWh)	Maximum Discharge		
Toyota Prius	11.3	384.4	4.4	90%	157.7	142.0
Camry Hybrid	17	578.3	1.6	90%	232.8	209.5
Chevy Volt	8.9	302.8	18.4	90%	128.6	115.7
Nissan Leaf	NA	NA	24	83%	20.0	18.4
Tesla Model S	NA	NA	85	83%	70.8	63.8

5. ENHANCING RESILIENCE OF INDUSTRIAL FACILITY THROUGH VEHICLE TO GRID OPERATIONS

5.1. Using EV for Vehicle-to-Grid Operations in extreme weather

After the onslaught of an extreme weather event like hurricane, the distribution system often suffers significant damages and the end customers get impacted because of blackouts or power shortage. Several instances can be quoted from the past such as hurricanes Ike, Irene that happened in the US in 2008 and 2011, respectively, causing severe damage to the power grid infrastructure (Mensah et al. 2015). Another example is when Hurricane Irma hit Florida in 2017, around 5.8 million homes and business units were affected without power supply (FleetCarma,2018). It is highly desirable that the power grid should withstand extreme weather events and continue to serve critical loads, such as hospitals, traffic lights, and banking systems. Powering essential facilities and infrastructure under extreme weather is essential to satisfying the basic human needs. Hence it is important to enhance the resilience of the grid such that it is able to withstand, survive or quickly recover from the disaster events.

Due to the climate change, it is expected that the future would likely see an increase in frequency and intensity of extreme weather events, including hurricanes and tornados (FleetCarma, 2018). To cope with this situation, EVs prove to be an alternative to helping build resilience in the power grid during natural disasters. EVs can store reasonable amounts of electric energy in batteries that can be discharged for urgent use. They provide a good source of reserving power storage and can be used to power households (vehicle-

to-home) and business entities (vehicle-to-building) in contingency thereby maintaining grid stability and reducing electricity cost in peak hours.

The popularity of EVs has been increasing around the world in the past decade. There are 360,800 plug-in electric vehicles (PEV) sold in the US in 2018 out of which 66% were battery electric vehicles (BEV) and 34% were plug in hybrid vehicles (PHEV) (EVvolumes, 2018). Figure 40 shows the PEV sale in 2018 by car model and manufacturer.

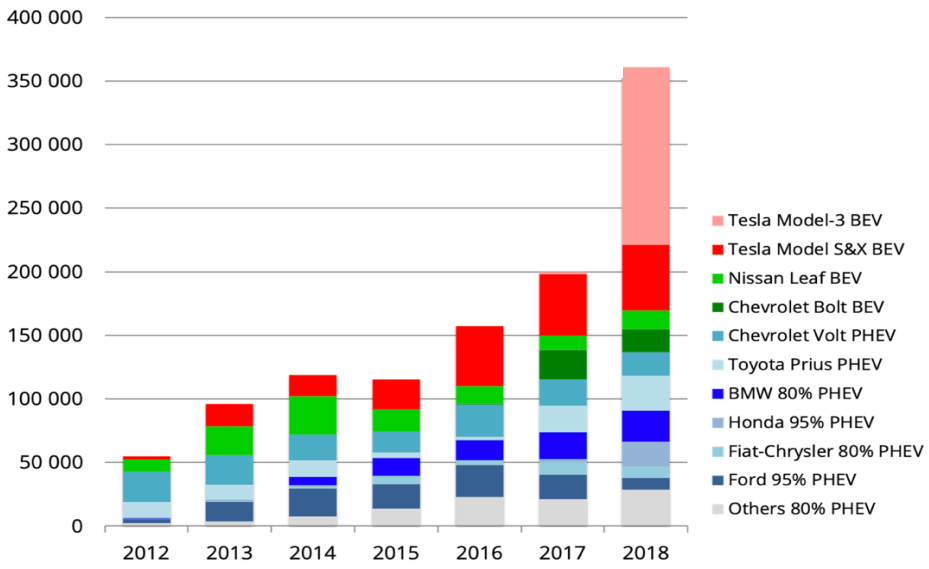

Figure 40. PEV sale in the US in 2018(EVvolumes,2018).

5.2. Enhancing Power Resilience of Industrial Facility through V2G Operations

5.2.1. Model setting

Most industrial facilities operate in 24/7 mode that consumes significant amounts of power across a year. An industrial facility is often connected to the main grid, or connected with a microgrid, or both. A microgrid system consists of wind turbine (WT), solar photovoltaics (PV), energy storage system (ESS), electric vehicle (EV) fleet, and factory load. Figure 41 shows the model setting of the industrial facility with the microgrid considered for our study.

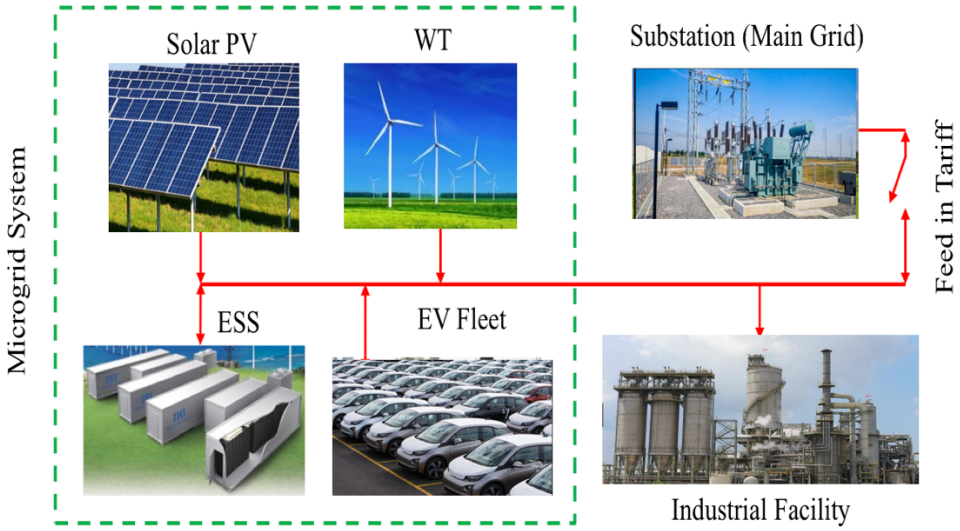

Figure 41. Microgrid set up of an industrial facility

During the normal operating condition, the energy from the microgrid is primarily used to meet the factory load. Any excess energy available can be used to charge the battery or sold to the grid under feed-in-tariff program. If the microgrid is not able to meet the factory load, power is purchased from the main grid in a utility rate. During an extreme event like a hurricane, a fleet of EVs are added in the microgrid to serve the factory demand due to the damage of the main grid. The research question in this chapter is to determine the siting and sizing of the microgrid system to ensure the power resilience at low cost. The decision variables are WT capacity (MW), PV capacity (MW), ESS capacity (MWh) and the EV fleet capacity (MWh). The objective function is to minimize the annualized energy cost under normal condition and extreme events. The latter pertains to the energy shortage cost of the industrial facility attacked by hurricane or other extreme weather events.

5.3. Model to calculate the cost under normal condition

Table 20. Notation for calculating cost under normal condition (N/A=not applicable)

Term	Description	Unit
$\underline{a_g}$	capacity cost for generation technology g	\$/MW
b_g	operation and maintenance cost for generation technology g	\$/MWh
c_g	carbon credits for generation technology g	\$/MWh
a_b	capacity cost for battery storage system	\$/MWh
ϕ_g	capital recovery factor of renewable generation technology g	N/A
ϕ_b	capital recovery factor of battery storage system	N/A
p	utility electricity rate	\$/MWh
q	feed-in-tariff rate	\$/MWh
L_t	energy demand of the facility in period t	MW
P_g^c	capacity of generation type g	MW
B^c	capacity of battery storage system	MWh
τ_{tg}	generation duration of generation type g	hours
$\lambda_{tg}(\zeta)$	power capacity factor at period t for generation type g	N/A
B_t	available energy of ESS at time t	MWh

During normal condition, the total available energy in the microgrid at time t is given by following equation.

$$E_t = \sum_{g=1}^{G} \tau_g \lambda_{tg}(\zeta) P_g^c + B_t \qquad \text{for } t=1, 2, \ldots, T \tag{5.1}$$

where

G is the number of generation types. Here, g=1 for WT and g=2 for PV

τ_{tg} is the generation duration, it could be 1 hour or several hours, depending on WT and PV. However, there is no PV generation in the night.

ζ is random climate condition at time t, for wind or weather condition.

$\lambda_{tg}(\zeta)$ is the power capacity factor at period t for generation type g, and $0<\lambda_{tg}(\zeta)<1$.

P_g^c is the capacity of generation type g.

B_t is the available energy of ESS at t, in that case B_t is positive. If B_t is negative, it means this amount of energy is charged into ESS.

Let C_1 be the cost under the normal operating condition, then

$$C_1 = \sum_{g=1}^{G} \phi_g a_g P_g^c + \phi_b a_b B^c + \sum_{t=1}^{T}\sum_{g=1}^{G} \tau_{tg}\lambda_{tg}(\zeta) P_g^c (b_g - c_g) + \sum_{t=1}^{T} \left(Pr\{E_t \le L_t\}\, p(L_t - E_t) - Pr\{E_t > L_t\} q(E_t - L_t) \right) \quad (5.2)$$

The first term represents the annualized installation cost of WT, PV and battery ESS. The second term represents the annual maintenance cost and carbon credits. The third term represents the payment of utility bill for taking power from the main grid and the revenue by selling surplus power to the grid.

5.4. Results and Observations

Table 21. Parameter values for normal operating condition

Term	WT	PV	Unit
b_g	8	10	\$/MWh
c_g	0	35	\$/MWh
a_b	1.5×10^6	1.5×10^6	\$/MWh
ϕ_g	0.08024		
ϕ_b	0.1295		
p	75		\$/MWh
q	35		\$/MWh
L_t	10		MW
τ_{tg}	8760		hours

For the analysis, we have assumed a factory load of 10 MW. The simulation is performed for a time period of one year (8760 hours). The capacity factor of WT, PV and their capacity cost vary to cover a wide operation range, and the results are analyzed. Table 21 provides the benchmark values for various parameters.

5.4.1. Effect of battery capacity cost on the system

If we assume the power capacity factor of Wind Turbine (WT) and Photovoltaics (PV) to be 1, and their capacity cost to be $1.5 M/MWh, it can be seen from Figure 42 that, the total system cost reduces as the Battery Storage System (BSS) capacity cost decreases. Also, the system choses to increase BSS capacity to meet the factory load. This is the most optimistic assumption because capacity factors of WT and PV can hardly reach 1.

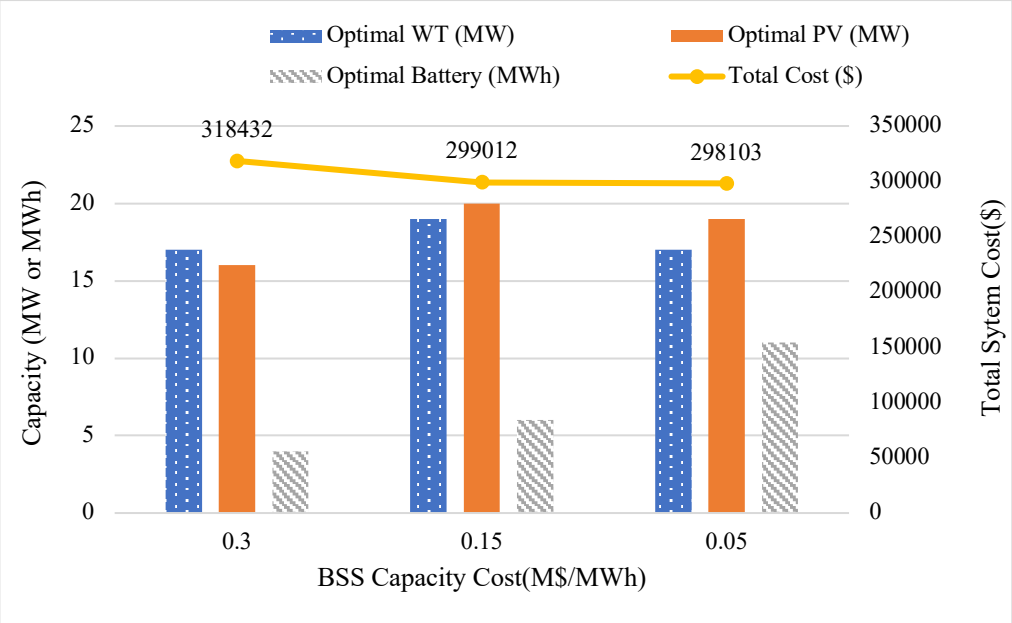

Figure 42. BSS capacity cost versus system cost -case I.

However, if the capacity factor of WT and PV are now reduced to 0.5, it can be seen that there is a need to install more WT and PV capacity to meet the factory load. In addition, the BSS capacity also increases considerably as it becomes more cost-effective in terms of

capacity cost. It is obvious that the total system cost is increased compared to the previous scenario.

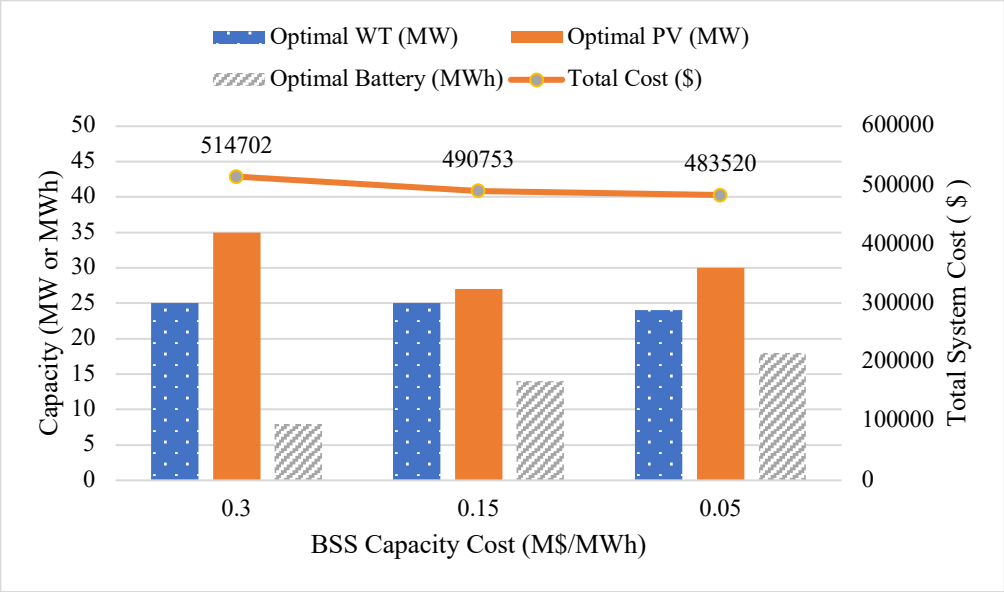

Figure 43. BSS capacity cost versus system cost -case II.

5.4.2. Effect of PV capacity cost on the system

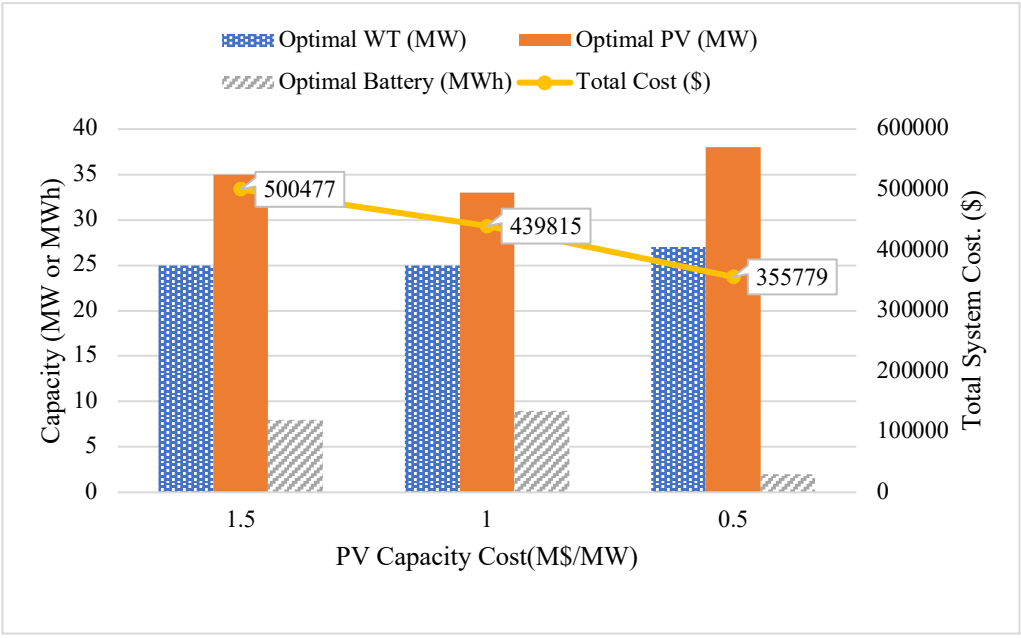

Figure 44. PV capacity cost versus system cost

For a capacity factor of 0.5 for both WT and PV and BSS capacity cost of $0.3 M/MWh, Figure 44 shows how the total system cost varies with respect to PV capacity cost. It can be seen that as the PV capacity cost goes down, its usage goes up. Also, the corresponding total system cost is lower compared to a reduced BSS capacity price. This is also due to the fact that PV has carbon credits associated with it.

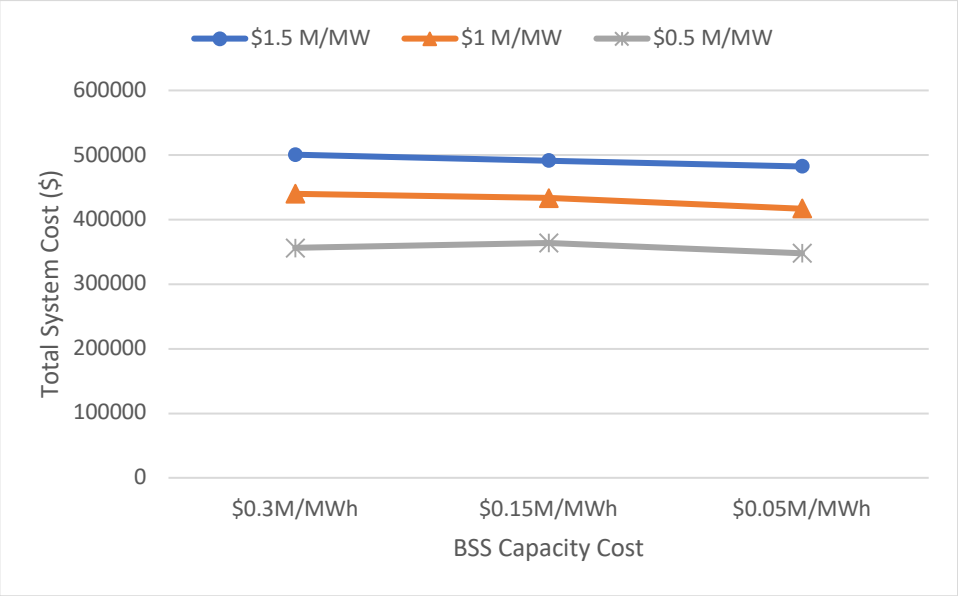

Figure 45. PV and BSS capacity cost versus system cost

The above figure shows how the system cost varies with BSS and PV capacity cost. It can be seen that for a fixed PV cost, even if we reduce the BSS capacity cost to less than half the original price, the total system cost saving is very meagre. However, if the PV capacity cost is reduced, there is a considerable reduction in the total system cost.

5.5. Model to calculate the cost under Extreme Weather Event

During an extreme weather event like a hurricane, the main grid could be completely down and there is no sufficient power to energize the industrial facility. In this situation, the industrial facility can operate in an island mode along with the microgrid consisting of PV, WT and BSS. As a benchmark, we have taken the time duration of the extreme

event to be 24 hours and the energy demand of the factory during the extreme event to be 240 MWh with average load of 10 MW. The other parameters and their notation are listed in Table 22.

Table 22. Parameters for calculating cost under extreme weather condition

Parameter	Description	Unit
τ_e	Duration of the extreme event	hours
$\lambda_{eg}(\zeta)$	Power capacity factor for generation type *g* during extreme event	N/A
P_g^c	Capacity of generation type g	MW
b_{eg}	Operation and maintenance cost in extreme event	$/MWh
c_{eg}	carbon credits in extreme event	$/MWh
π	The manufacturing downtime cost due to energy shortage	$/MWh
L_e	Energy demand of the facility during the extreme weather condition	MWh
E_e	Output power of microgrid including V2G during extreme event	MWh
ω	The cost for paying the V2G service	$/MWh
N_e	Number of EV participating in the V2G program during extreme event	number
E_{ev}	Energy contributed by a single EV during extreme event	MWh
B_e	The available energy of ESS at the beginning of extreme event	MWh

The cost under extreme event, denoted as C_2, is comprised of the industrial facility production loss due to power shortage, and the cost of using V2G services. During the extreme event, we assume that WT and PV generation may not fully available because of

the adverse weather condition, hence the output of WT and PV is scaled down. The output power of microgrid including V2G program during the extreme event becomes

$$E_e = \sum_{g=1}^{G} \tau_e \lambda_{eg}(\zeta) P_g^c + B_e + N_e \times E_{ev} \tag{5.3}$$

where

τ_e=the duration of the extreme event in unit of hours.

ζ=random climate condition in extreme condition.

$\lambda_{eg}(\zeta)$=power capacity factor for generation type g during extreme event.

B_e=the available energy of ESS at the beginning of extreme event and B_e could be positive or zero. Since in extreme event, the power generation is in shortage, there is no excessive power for recharging the ESS.

N_e=number of EV participating in the V2G program during extreme event, and it could be a random variable.

E_{ev}=energy contributed by a single EV during extreme event, and it could be a random variable.

Now the energy cost during the extreme event is given by,

$$C_2 = \sum_{g=1}^{G} \tau_e \lambda_{eg}(\zeta) P_g^c (b_{eg} - c_{eg}) + \pi\left(L_e - E_e\right) + \omega N_e E_{ev} \tag{5.4}$$

In above equation, the first term represents the net cost. This is comprised of operation and maintenance (O&M) cost and the carbon credits during the extreme event period. The O&M during extreme event is likely higher than in the normal condition because of the protection of WT and PV or potential damages for repair. The second term is the energy shortage cost, and the third term is the cost for adopting the V2G service. The total cost is the sum of C_1 and C_2 and is given by the following equation.

$$C_{total} = C_1 + C_2 \tag{5.5}$$

5.6. Result Analysis and Discussion

During an extreme weather event, the EV fleet provides additional power to the factory. We assume a microgrid comprised of a fleet of EVs along with the WT, PV and BSS in contingency. The following table lists the benchmark values assumed for the extreme event simulation.

Table 23. Parameter values for Extreme Event Condition

Parameter	WT	PV	Unit
$\lambda_{eg}(\zeta)$	0.2	0.1	
b_{eg}	100	80	\$/MWh
c_{eg}	0	35	\$/MWh
τ_e	24		hours
π	5000		\$/MWh
L_e	10		MW
ω	1000		\$/MWh
N_e	100		number
E_{ev}	40(Nissan Leaf Second Gen.)		MWh
B_e	50		Percentage

5.6.1. Effect of EV fleet size on the cost

During the extreme event, the WT, PV and BSS alone may not be able to meet the factory demand, therefore we include EV fleet to compensate for the potential energy shortage. Figure 46 shows that as the EV fleet size increases, the energy supplied is close to the factory demand of 240 MWh and at the same time the levelized cost of electricity (LCOE) also decreases. LCOE is defined as the ratio of the total energy cost over the total energy

used during the course of a year. There is an 87% decrease in the LCOE when the fleet size increases from 100 to 3000. This is because the production loss due to power shortage is greatly reduced.

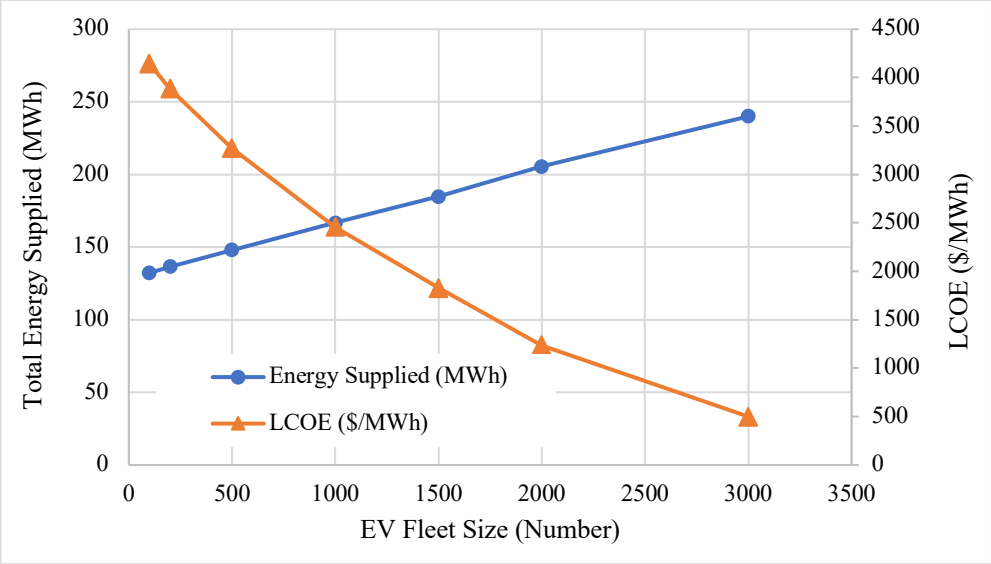

Figure 46. EV fleet size versus LCOE during extreme event

5.6.2. Effect of production loss due to power shortage

The production loss of the factory due to power shortage is the cost incurred due to decreased production capacity during the extreme event. This value is usually denoted in dollars per MWh and increases if the factory load is not met by available power. From Figure 47 it can be seen that for a given V2G service cost of $1000/MWh, the LCOE increases steeply with the rise in the production loss. It can be observed that there is a 78% increase in the LCOE when the production loss increases from $1000/MWh to $5000/MWh.

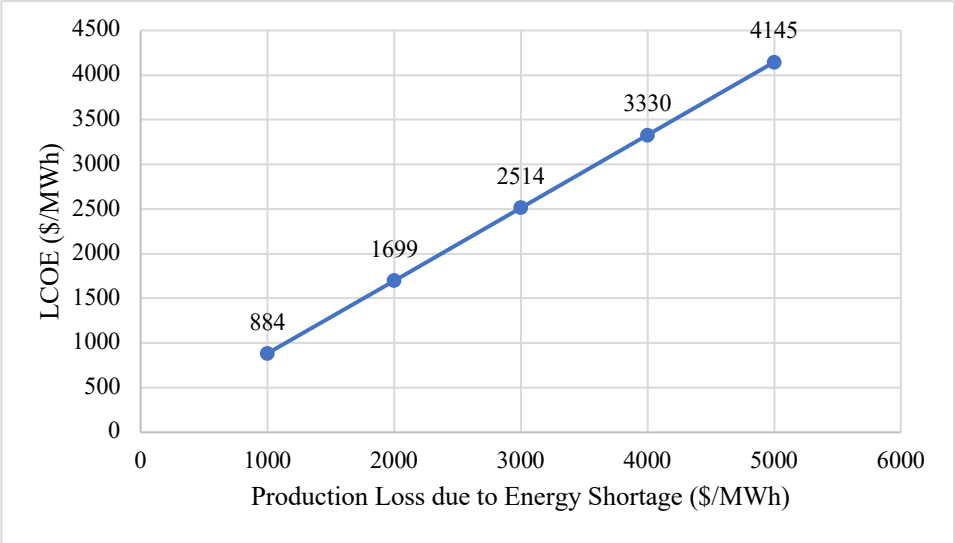

Figure 47. Production loss versus LCOE during extreme event

5.6.3. Effect of V2G service cost

During the extreme event, there is a V2G service cost that should be given to all EVs who have participated in the V2G program. For a given production loss of $1000/MWh, we observe how the LCOE varies with respect to change in V2G service cost. It can be seen from Figure 48 that the LCOE increases slightly as the V2G service cost increases, but not as much as compared to an increase in the production loss. There is only a 2.8% increase in the LCOE when the V2G service cost increases from $1000/MWh to $5000/MWh. This is much lower compared to the 78% increase in the previous case.

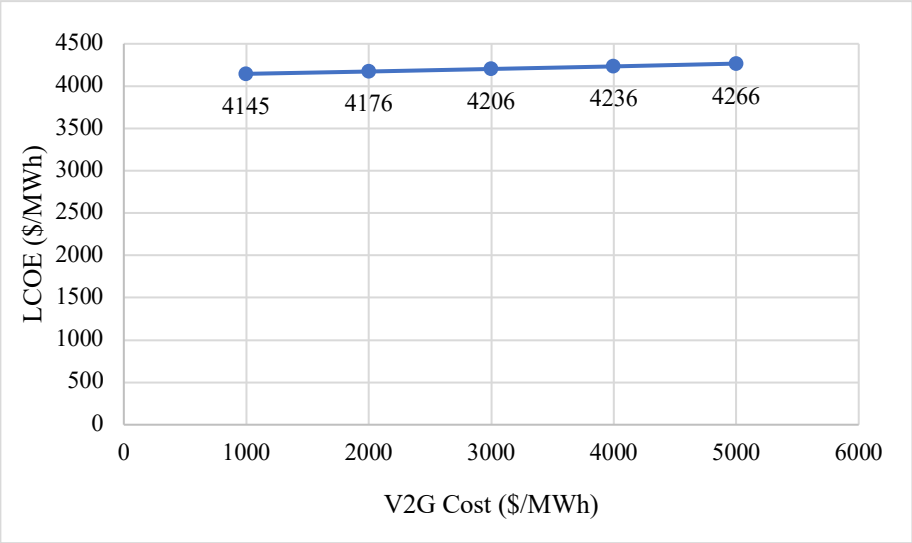

Figure 48. V2G service cost versus LCOE during extreme event

5.7. Total Annual System Cost

In order to calculate the total system cost, we run the simulation for one year assuming a hurricane occurrence rate of 0.001. We use Poisson distribution to generate the random occurrence of the hurricane. The simulation calculates the normal cost during the entire year and when the event occurs, the system cost is calculated under the extreme condition.

For the normal scenario, we consider a capacity factor WT and PV as 0.5. The capacity cost for WT and PV as $1.5M/MW and the battery capacity cost to be $0.3 M/MWh. For the extreme scenario, we consider the capacity factor of WT and PV to be 0.2 and 0.1 and the charge on the BSS to be 50% of its capacity. We consider Nissan Leaf second generation fleet of EVs which have a battery capacity of 40 kWh. The factory load is assumed to be 10 MW. Table 24 provides the LCOE values for different scenarios.

Table 24. The values of LCOE in various scenarios

No of EVs in the fleet	V2G Service cost ($/MWh)	Production Loss (π) ($/MWh)	LCOE ($/MWh)
100	1000	5000	57.55
500	1000	5000	58.10
2000	1000	5000	64.4
100	1000	2000	56.4
500	1000	3000	58.10
500	1000	2000	50.58
100	2000	5000	56.85
1000	3000	5000	70.5
3000	1000	5000	68.72
1000	1000	4000	60.5
100	1000	3000	56.4

It can be seen from the above table that the number of EVs in the fleet, V2G service cost and the production loss have a significant effect on the LCOE of the total system. The rise in any of these parameters affects the LCOE directly. The minimum LCOE in the table is $50.58/MWh, and the maximum is $70.5/MWh. The difference is $19.92/MWh, or nearly 40% of the lowest LCOE.

6. CONCLUSION AND FUTURE WORK

6.1 Summary of the thesis

In this research the problem of improving power grid resilience post an extreme event is analyzed and studied. The work is broadly split into two parts. The first part of the thesis comprised of Chapters 2 and 3 focuses on analyzing Hurricane Harvey's aftermath and the factors that govern the recovery process post the event. In the second part of the thesis comprised of Chapters 4 and 5, we discuss how to improve the resilience of an industrial facility with minimum operational cost post an extreme event with V2G as a potential resource. The contribution of each chapter along with its uses and future work is discussed in detail below.

Chapter 2 aims at modeling the extreme weather events like hurricanes, flooding and earthquakes that lead to a majority of the power outages. The simulation of a hurricane developed using MATLAB helps us to understand the impact these High Impact Low Probability Events (HILP) have on the economy and critical infrastructures like power grid. It also gives us an idea of the radius of geographical area that will be affected for different categories of hurricanes. The storm surge model enables us to calculate the equipment failure rate for various hurricane categories. The earthquake model gives us useful information about the frequency of occurrence of an earthquake, its magnitude and peak ground acceleration, and released energy in difference scale.

Chapter 3 discusses in detail about the repair and recovery models of transmission lines and its application to Hurricane Harvey. Based on the early work of Jin et al. (2018), the idea of applying Markov chain model for the repair and recovery of transmission and distribution lines is further expanded in terms of system scope and complexity. We utilize

the power outage data released by ERCOT post Harvey to arrive at the failure rate and repair rate. With this data, we perform sensitivity analysis and analyze how various parameters like repair rate, failure rate, number of transmission lines and repair teams have on expected number of failed lines (L), average number of failed lines waiting to be repaired (L_q), expected recovery time (W) and average waiting time for repair for a failed line (W_q). This work can be extended in the future to develop repair and recovery models for other outdoor electrical components such as transformers, generators, and circuit breakers, and perform sensitivity analysis for them.

In Chapter 4, we discuss about the various Electric Vehicles (EVs) available in the market and develop a mathematical model for the EV Battery swap process using Erlang B queuing model. Apart from the various commercial charging topologies available in the market today, we have also included supercharging technology by Tesla. We analyzed how the required number of spare batteries for various EVs vary at different EV arrival rates and blocking probabilities for different charging levels. This work can be extended in the future by applying other queuing models that will resemble more real-life situations. In addition to this, we also discuss how to calculate the energy and power available from a BEV and HEV and have presented this data for some EVs available in the current market. This data will be useful in knowing how much energy could be discharged from a fleet of EVs when they are used during contingencies for V2G applications to power critical power infrastructure.

In Chapter 5 we discuss how the power resilience of an industrial facility can be enhanced using V2G operation. We set up a model of an industrial facility with a microgrid consisting of WT, PV, BSS and a fleet of EVs. We calculate the system cost

during normal operation and analyze how it varies for different capacity factors of WT and PV and for varying capacity costs for WT, PV and BSS. This study helps us to perform optimum sizing and siting of WT, PV and BSS to ensure power resilience at minimum total system cost. We also calculate the system cost during contingencies when the main grid is cut off and the industrial facility is powered by EV fleet and the microgrid alone. We analyze how the EV fleet size, the V2G service cost and the production loss cost affect LCOE of the facility. The results from this study are useful in finding out the optimum number of EVs in a fleet to ensure power resilience at minimum system cost. Finally, we perform a one-year hourly simulation and calculate the LCOE for different scenarios for a given hurricane occurrence rate. This gives us useful information about how the LCOE gets affected by various parameters such as EV fleet size, manufacturing production loss and V2G service cost.

6.2 Future research directions

The research can be extended in the future to the design phase and the operation phase of power grid for its resilience enhancement. Areas such as topology/network reconfiguration post an extreme weather event, distributed generation integration (DG) to enhance power grid resilience can be explored. Microgrid operation of DGs to help build resilience of the system after the failure of the conventional grid could also be studied. Another potential area of study is the integration of prosumers with microgrid to enhance resilience of industrial facility. Many industrial factories including commercial buildings now have their own microgrid comprising of roof-top PV, onsite WT, and EV fleet. During emergency situations these prosumers could provide power to critical power

infrastructures or realize self-supply of energy through island microgrid generation or V2G operations.

Mathematical modeling and data mining techniques such as artificial neural networks and other machine learning algorithms could be used to model Categories 4 and 5 hurricanes to study and analyze various factors that govern recovery process. This data might be useful in preparing us to face these extreme events in the future. In addition, this can also be extended to other extreme weather events like snowstorms, forest fires, freeze, etc. For areas that are more prone to certain types of extreme weather event, cost effective hardening measures could be carried out during the early design and development phase of grid with the help of these models.

The electrical grid serves as the backbone of the economy. A well-designed electrical grid should be able to minimize the number of power interruptions and quickly recover from a disaster event. It becomes the need of the hour to have emergency preparedness as many extreme weather events have uncertainties associated with them. Fast recovery plays an important role in making a power system more resilient and helps prevent unwarranted expenses and operational losses. This calls for incorporating smart operational measures that can improve controllability, flexibility and observability of a power system in response to an extreme event. Some of the measures include decentralized control with distributed energy systems, microgrids, adaptive wide area protection and control schemes, advanced visualization and situation awareness systems and disaster response and risk management techniques.

APPENDIX SECTION

APPENDIX A Simulation of a Hurricane

```
clear

%Hurricane occurence with poisson(years)
lambda=0.29677; % unit is event per year

occurence=-log (1-rand ())/lambda
occurence_hrs=occurence*365*24
%Approach angle with binormal(degrees)

mu1=35;
sigma1=25;
mu2=295;
sigma2=40;
a1=0.5;
z=sqrt (-2*log (rand ())) * sin (2*3.14*rand ());
theta1=mu1+(sigma1*z);
theta2=mu2+(sigma2*z);
theta=(a1*theta1) +((1-a1) *theta2);

disp('approach angle in degrees')
theta

%Hurricane translational velocity with lognormal (meters per second)

mu=2.3+((-0.00275) *theta);
sigma=0.3;

Translational_speed=lognrnd(mu,sigma);
disp('Translational velocity in metres per second')
Translational_speed

% Hurricane central pressure difference at landing with weibull(millibar)
%lambda=a=c & k=b
c=35-(0.1*theta); % 0.1 is taken to keep c poistive.
k=1.15;
disp('central pressure difference at landing')
delta_po=c*(-log (1-rand ())) ^ (1/k)

% minimum central pressure at landfall(millibar)

atm_pressure=1013;
central_pressure=atm_pressure- delta_po;
```

```
disp('Central pressure at landing in millibar')
central_pressure

%central pressure filling rate
a4=0.006;
a5=0.00046;
epsilon=0.025;


a=a4+(a5*delta_po) + epsilon;
for t=1:72
   delta_p(t)=delta_po*exp(-a*t);

end
disp('Central Pressure Filling Rate for 72 hours')
delta_p

%radius to maximum wind speed
psi=25.9; %storm latitude
disp('radius to maximum wind speed in kilometres')
ln_R_max=2.556-(0.000050*delta_po * delta_po) + (0.042243032*psi);
Radius_to_max_wind_speed=exp(ln_R_max)


%wind speed decay rate (metres per second)
Vb=13.75;
r=0.9;
alpha=0.095/3600;
Vo=1.287;


for t=1:72

v(t)= Vb+((r*Vo)-Vb) * exp(-alpha*t);
end
disp('Wind speed decay rate in metres per second')
```

APPENDIX B Markov Model for transmission and distribution lines

```
% This program is the Markov Chain model for transmission and distribution
% lines for the case of Hurricane Harvey.
%Last Updated: August 5 ,2019.
clear
K=200
R=30
lambda=1.84
mu=1.0250
c=zeros (1, K+1)
pi=zeros (1, K+1)
c (1) =1;

%CALCULATING LAMBDA AND MU
for i=1: K
l(i)=(K-i+1) *lambda

if i<=R
  mui(i)=i*mu
else
   mui(i)=R*mu
end

end

%CALCULATING C
for i=2:(K+1)
   c(i)=c(i-1) * l(i-1)/mui(i-1)
end

%compute pi

check=sum(c) %to check if the value of c becomes infinity
pi (1) =1/sum(c)
for k=2:(K+1)
   pi(k)=c(k)* pi (1)
end

%computing (L)- Expected number of damaged branches
l=zeros (1, K+1)
l(1)=0
for n=2:(K+1)
   l(n)=pi(n)*(n-1) %since pi(n) needs to be multiplied by the (n-1)th state
end
 L=sum(l)
```

```
%computing (Lq)-Avg number of lines waiting to be repaired
lq=zeros (1, K+1)
for k=1:(K+1)
   if k<R
      lq(k)=0
   else
      lq(k)=pi(k)*(k-1-R) %since pi(k) needs to be multiplied by the (n-1)th state
   end
end
Lq=sum(lq)

%comuputing (Ls)-Avg number of lines under service
Ls=L-Lq

%calculating lambdabar
a=zeros (1, K+1)
a(K+1) =0
for i=1: K
   r=K
   a(i)=lambda*r
   K=K-1
end
q=zeros (1, K+1)
q(K+1) =0

for t=1:200

   q(t)=a(t)* pi(t)

end

tot_lambdabar=sum(q)

%computing (W)-Duration of recovering a damaged branch
W=L/tot_lambdabar
%computing (Wq)-Avg wait time in the queue
Wq=Lq/tot_lambdabar
%computing (Ws)-Avg time a line is under repair
Ws=W-Wq
```

APPENDIX C Erlang B Model for Electric Vehicle Battery Swap Process

```
% This program is the Erlang B Model for an EV Battery Swap Process.
%Last Updated: August 5,2019.
clear
lambda=5;
mu=0.0825;
s=60;
c=zeros (1, s+1);
pi=zeros (1, s+1);
rho=lambda/mu
mui(1)=mu

%calculating lamda and m for all states
for j=1:(s+1)
   l(j)=lambda
end

%calculating mu for all states
n=2;
for j=2:(s+1)
  mui(j)=n*mu
  n=n+1
end

%calculating cj for all states
c (1) = 1
for j=2:(s+1)
   c(j)=(rho^(j-1))/factorial(j-1)
end

%calculating pi for all states
pi (1) =1/sum(c)
for i=2:(s+1)
   pi(i)=pi (1) *c(i)
end

%calculating pi(s)
pis=c(s+1) * pi (1)
blocking_prob_percentage=pis*100;
%calculating L,Ls,W,Wq
L=rho*(1-pis)
W=1/mu
```

APPENDIX D Normal Operating Cost of an Industrial Facility with a microgrid

```
% this code is developed for simulating the facility power resilience
% during extreme weather event.
% The codes consist of two parts: cost under normal operating
% condition(totalcost.m) and cost under extreme event(extremecost.m).
% last updated on June 30, 2019

%initializing Test variables

    clear

    %simulating one hurricane for one year using Poisson Distribution
    lambda = 0.0001; % Events per hour- in reality 0.0001
    event_start = floor(-log(1-rand())/lambda); % Random occurence of hurricane in a year


    minC1= 10^20;
    minC2= 10^20;
    cost_normal=0;
    cost_extreme=0;
    % Setting delta values for WT, PV and BT

    d_WT=1; % incremental step size of WT
    d_PV=1; % incrmental step size of PV
    d_BT=1; % incremental step size of battery

    LCOE_1 = 0;
    LCOE_2 = 0;
    %major test variables for normal operating condition
    capcost_WT = 1.5 * 10^6; %captital cost of WT per MW
    capcost_PV = 1.5 * 10^6; %capital cost of PV per MW
    capcost_BT = 0.3 * 10^6; %capital cost of battery per MWh

    %inialize the major test result variables
    WT_op=0;
    PV_op=0;
    BT_op=0;

    powercapfactor_WT = 0.5; %maximum power capacity factor of WT
    powercapfactor_PV = 0.5; %maxium power capacity factor of PV

    Bg_PV = 8; %O&M cost for PV in $/MWh
    Bg_WT = 10; %O&M cost for WT in $/MWh
```

```
   Ln = 10; % Factory hourly electric demand during normal operating condition in MW

%--------Main program Æ %--------

   BT=-d_BT; % BSS capacity for each iteration
   for k=1:40
       BT= BT+d_BT;

      PV=-d_PV; % PV capacity for each iteration
      for i=1:40
         PV=PV+d_PV;

         WT=-d_WT; % WT capcity for each iteration
         for j=1:50
            WT=WT+d_WT;

            %calculating the first term of the annualized capacity or installation cost
            Fc = FixedCost(PV, WT, BT, capcost_PV, capcost_WT, capcost_BT);

            %Calculating the annual cost on hourly basis
            Ac = CostAnnual(WT, PV, BT, powercapfactor_PV, powercapfactor_WT,
Bg_PV , Bg_WT, Ln, event_start);

            %calculating annual operating cost in normal condition
            cost_normal = CostNormal(Fc, Ac);

      %--------Finding the optimum WT, PV and BT values for the normal operating cost
            if cost_normal<minC1
               minC1 = cost_normal;
               WT_op=WT;
               PV_op=PV;
               BT_op=BT;

               LCOE_1 = (minC1)/(8760*Ln); %the 8760*Ln representing the total energy
use of the facility in a year
            end
         end
      end
   end

   D =['The optimized values for normal condition are WT = ',num2str(WT_op), ' MW,
BT = ',num2str(BT_op),' MWh, PV =',num2str(PV_op),' MW',newline ' Minimum cost=
',num2str(minC1),' dollars', ' , LCOE= ',num2str(LCOE_1), ' $/MWh' ];
   disp(D)
```

```
%--------End of main program. Fuctions are defined below%--------

%Calculating total normal cost
function Cn = CostNormal (T1, T2)

   Cn = T1 + T2;

end

%term 1 of normal cost calculation
function Fc = FixedCost(P1c , P2c , P3c, capcost_PV, capcost_WT, capcost_BT)

   caprec = 0.08024/20; % capital recovery factor of WT and PV over 20 years
   caprec_BT = 0.1295/10; %capital recovery factor of BT over 10 years
   Fc = ( caprec * capcost_PV * P1c ) + ( caprec * capcost_WT * P2c )+(caprec_BT *
capcost_BT * P3c);
end


% term 2 of normal cost calculation
function AnnualCost = CostAnnual(WT , PV , BT , powercapfactor_PV,
powercapfactor_WT, Bg_PV, Bg_WT, Ln, event_start)

   T2total = 0;
   T3total = 0 ;
   Gt = 0;
   T2 = 0;
   Bt = 0; % Battery stored energy initially is zero.
   p = 75; %utility rate (p=75 $/MWh)
   q= 35; %feed in tarrif rate (q= 35 $/MWh)

   carbcredits_WT = 0; %carbon credits for WT
   carbcredits_PV = 35; %carbon credits for PV

   %Generating random power factor for WT and PV for one year on hourly
   %basis
   t=1;
    while t<= 8760
%       if t == event_start %Goto extreme event cost calculation module when the
extreme event starts
%          extremecost;
%          t = t + 24; % Offset time to contine after the extreme event which happens for
24 hours
%       else
         t=t+1;
%       end
```

```
WT_randCF = powercapfactor_WT * rand();  % here we use "WT_randCF" for hourly random capacity factor of WT
PV_randCF = powercapfactor_PV * rand();  % here we use "PV_randCF" for hourly random capacity factor of PV
if (((WT * WT_randCF) + (PV * PV_randCF)) - Ln) < (0.25 *Ln)%condition to ensure min.cost > revenue

T2 = ( 1 * WT_randCF * WT * (Bg_WT - carbcredits_WT) )+( 1 * PV_randCF * PV *( Bg_PV - carbcredits_PV ) );

%calculating the third term for one year on hourly basis

 Gt = (WT * WT_randCF) + ( PV * PV_randCF ); % this is the total hourly power from WT and PV
   % The first scenario- generation > demand

   E_maingrid=0 ; % define energy to main grid or taken from the main grid in an hour

   if Gt > Ln
      if Bt < BT  % battery is not fully charged scenario
         x= BT - Bt ;
         if (Gt - Ln)>= x
            Bt = BT; % Battery cap should be max since Battery should be fully charged.
            E_maingrid= Gt - Ln - x ; % this is the suplus power fed into the main grid
         else
            Bt = (Gt - Ln) + Bt;  % charge battery upto whatever excess energy is available without exceeding the BT capacity
            E_maingrid=0 ; % no suplus power fed into the main grid because the battery fully takes the extra power from WT and PV
         end
      end
   end

   % The second case scenario - generation < demand
   if Gt < Ln
      y= Ln - Gt;
      if (Bt > 0) && (Bt > y) % if the battery has charge available then use it for the deficit else battery will be drained completely
         Bt = Bt - y; % battery discharge energy to the facility
         E_maingrid=0; % no need of taking the power from main grid because the power shortage is met by the battery
      else
```

```
                E_maingrid=Bt-y; % this is the energy taken from the main grid (notice it is
"-" sign
                Bt = 0; % the battery is emptied because all its available energy is discharged
to the facility
            end
        end

        % calculating total availabale energy in grid at time t

        if E_maingrid <= 0
            T3 = p * abs(E_maingrid); % since power shortage, importing the power from
the main grid, it is a cost to facility
        else
            T3 = q * (-E_maingrid); % since it sells surplus power, the cost is negative
        end

        T3total = T3total + T3; %summation of Third term over time t
        T2total = T2total + T2; %summation of T2 for every hour upto 8760 hours
        AnnualCost = T2total + T3total; % SECOND TERM + THIRD TERM
    end
  end
end
```

APPENDIX E Vehicle to Grid based Operating Cost of an Industrial Facility during an extreme weather event

```
%initializing Test variables
%    clear
  minC2= 10^20;
  cost_extreme=0;

   % Setting delta values for WT, PV and BT
   d_WT=1.0;
   d_PV=1.0;
   d_BT=1.0;

   LCOE_2 = 0;

   %major test variables for normal operating condition
   capcost_WT = 1.5 * 10^6; %captital cost of WT
   capcost_PV = 1.5 * 10^6; %capital cost of PV
   capcost_BT = 0.3 * 10^6; %capital cost of

   %major test result variables

   WT_op_ext=0;
   PV_op_ext=0;
   BT_op_ext=0;

   powercapfactor_WT_ext = 0.2; %Power capacity factor of WT in extreme weather
   powercapfactor_PV_ext= 0.1; %Power capacity factor of PV in extreme weather
   BT_charge = 0.5; % Percentage of battery charge before the start of extreme event

   Bg_PV_ext = 80; %O&M cost for PV in Extreme weather (Taken as 10 times the
normal cost) $/MWh
   Bg_WT_ext=100; %O&M cost for WT in Extreme weather-$/MWh
   ProdLossCost = 5000; % Production Loss Cost -$/MWh

   Time_ext = 24; %Duration of the extreme event in hours
   Ln = 10; % Factory Power Demand during normal operating condition in MW
   Le = Ln * Time_ext; % Factory Energy Demand during the entire contingency period
in MWh

   %V2G variables declaration and initialization
   Ne = 100; %no. of EVs participating in V2G
   Eev = 40/1000; % energy contributed by a single EV in MWh, Nissan Leaf = 24 kWh

% incrementing PV, BT and WT generation capacity by delta
```

```
%--------Main program %--------

   BT=-d_BT; % BSS capacity for each iteration
   for k=1:240
       BT= BT+d_BT;

      PV=-d_PV; % PV capacity for each iteration
      for i=1:240
         PV=PV+d_PV;

         WT=-d_WT; % WT capcity for each iteration
         for j=1:240
            WT=WT+d_WT;

       %------cost under extreme events-------

             % calculating first term under extreme events
             T1e = firstterm_extreme (WT, PV,Bg_PV_ext ,Bg_WT_ext ,Time_ext ,
powercapfactor_WT_ext , powercapfactor_PV_ext );

             % calculating second term under extreme events
             [T2e, test] = secondterm_extreme (PV, WT, BT, Time_ext, Ne, Eev, Le,
powercapfactor_WT_ext, powercapfactor_PV_ext, BT_charge, ProdLossCost);


             % calculating the third term under extreme events
             T3e = thirdterm_extreme (Ne, Eev);

             %calulation total cost under extreme events

             cost_extreme = TotExtremeCost (T1e, T2e, T3e);
      %--------Finding the optimum WT, PV and BT values for the Extreme event
operating cost---------
       if test == 0 %calculate minimum cost only when demand is greater or equal to
supply
            if cost_extreme<minC2
               minC2 = cost_extreme;
               WT_op_ext=WT;
               PV_op_ext=PV;
               BT_op_ext=BT;
               Total_energy_supplied = (WT_op_ext * powercapfactor_WT_ext) +
(PV_op_ext * powercapfactor_PV_ext) + (BT_op_ext * BT_charge) + (Eev * Ne);
               EnergyDifference = (Le - Total_energy_supplied);
               TotProdLoss = (EnergyDifference * ProdLossCost);
               LCOE_2 = (minC2 + TotProdLoss)/Total_energy_supplied; %since it is for
one year on hourly basis
```

```
            end
        end

        end
    end
end


 E =['The optimized values for extreme condition are WT = ',num2str(WT_op_ext), '
MW, BT = ',num2str(BT_op_ext),' MWh, PV =',num2str(PV_op_ext),' MW',  ', EV =
',num2str(Ne*Eev) , 'MWh',newline ' Min. cost = ',num2str(minC2),' dollars', ',  LCOE = '
,num2str(LCOE_2),' $/MWh',', Total Energy Supplied = '
,num2str(Total_energy_supplied), ' MWh'];
 disp(E);

% end of the main program

% term 1 of extreme event
function T1ext = firstterm_extreme (WT, PV, Bg_PV_ext, Bg_WT_ext,Time_ext,
powercapfactor_WT_ext, powercapfactor_PV_ext)

   T1ext = (Time_ext * powercapfactor_WT_ext * WT * (Bg_WT_ext - 0)) + (Time_ext
* powercapfactor_PV_ext * PV *(Bg_PV_ext - 35));
end


% term 2 of extreme event
function [T2ext, test] = secondterm_extreme (PV, WT, BT, Time_ext, Ne, Eev, Le,
powercapfactor_WT_ext, powercapfactor_PV_ext, BT_charge, ProdLossCost)
   test = 0;
   T2ext = 0;
   V2G_energy = 0; %Energy from EVs
   Energy_deficit = 0;
   Be = BT_charge * BT; % Energy available in the storage battery before extreme event
starts

   E_grid = (Time_ext * ((powercapfactor_WT_ext * WT) + (powercapfactor_PV_ext *
PV)) + Be); % energy from WT, PV and BT alone for each iteration
   V2G_energy = (Ne * Eev); %Energy from EVs
   Energy_deficit = (Le - V2G_energy); % Calculate the deficit energy from V2G to meet
the factory demand
        if E_grid <= Energy_deficit
           Ee = E_grid + V2G_energy; %calculating the energy available in the grid
+V2G Energy
           T2ext = ProdLossCost * (Le - Ee);
             if T2ext < 0 % condition to catch a situation where supply exceeds demand
```

```
                test = 1;
                end
        end
end


% third term of extreme event
function T3ext = thirdterm_extreme (Ne, Eev)

    w = 2000; %cost for V2G service in dollars per MWh
    T3ext = w * Ne * Eev; %T3ext is the cost for V2G service

end

%Total cost of extreme event

function totalcost = TotExtremeCost (t1, t2, t3)

    totalcost = t1 + t2 + t3;

end
```

REFERENCES

Arab, A., Khodaei, A., Khator, S., Ding, K., Emesih, V., Han, Z., (2015), "Stochastic Pre-hurricane Restoration Planning for Electric Power Systems Infrastructure", IEEE Transactions on Smart Grid, vol.6, no 2, pp. 1046-1054.

Babaei, S., Zhao, C., Ding, T., (2017), "Allocating Distributed Generators for Resilient Distribution systems under uncertain probability distribution of natural disasters", IEEE Power and Energy Society General Meeting,16-20th July 2017, Chicago, IL, USA.

Blaabjerg, F., Yang, Y., Yang, D., Wang, X., (2017), "Distributed power generation-Systems and protection", Proceedings of the IEEE, vol. 105, no.7, pp. 1311-331.

British Geological Survey, "Earthquake magnitude calculations," available http://www.bgs.ac.uk/discoveringGeology/hazards/earthquakes/magnitudeScaleCalculations.html, (accessed on Oct 1,2018)

Buque, C., Chowdhury, S., (2016), "Distributed Generation and Microgrids for Improving Electrical Grid Resilience: Review of the Mozambican Scenario" IEEE Power and Energy General Meeting (PESGM), 17-21st July 2016, Boston, MA, USA.

Che, L., Khodayar, M., and Shahidehpour, M., (2014), "Only connect: Microgrids for distribution system restoration," IEEE Power and Energy Magazine, vol. 12, no. 1, pp. 70–81.

Chester, C., Montoya, D., Flores, J., Jin, T., Jimenez, J., (2015)," An Overview of Electric Transportation and its Potentials in Industrial Demand Response", Proceedings of ISERC Conference, Nashville, TN.

Clements, D., Mancarella, P., (2017), "Fragility Curve based storm modelling of distribution networks with staff constraints", IET International Conference on Resilience of Transmission and Distribution Networks (RTDN 2017), 26-28th September 2017, Birmingham, UK.

Cox, W., Considine, T., (2014), "Grid Fault Recovery and Resilience: Applying structured Energy and microgrids", ISGT 2014, 19-22nd February, Washington DC, USA.

Dehghanian, P., Aslan, S., Dehghanian, P., (2017), "Quantifying power system resiliency improvement using network reconfiguration ", IEEE 60th International Midwest Symposium on Circuits and Systems (MWSCAS), 6-9th August 2017, Boston, MA, USA.

Electric light and power, (2018), "US to investigate power restoration efforts in Peurto Rico" available on https://www.elp.com/articles/2018/04/us-to-investigate-power-restoration-efforts-in-puerto-rico.html (accessed on November 8,2018)

ERCOT, (2018), “ERCOT responds to Hurricane Harvey,” Sept. 6, 2017, available http://www.ercot.com/help/harvey (accessed on November 8,2018).

Espinosa, A., Moreno, R., Lagos, T., Ordonez, F., Sacaan, R., Espinoza, S., Rudnick,H., (2017), “Improving Distribution Network Resilience Against Earthquakes,” International Conference on Resilience of Transmission and Distribution Networks, 26-28th September 2017, Birmingham, UK.

EV Volumes.com, (2018), titled “USA Plug in Sales for 2018 Full year” available “http://www.ev-volumes.com/country/usa/”, (accessed on May 21,2018)

FEMA, (2018), “Coastal Flood Risks: Achieving Resilience Together” available on https://www.fema.gov/coastal-flood-risks-achieving-resilience-together (accessed on Oct 5,2018)

Fleetcarma, (2018), titled “How Electric Vehicles could be used to Future Proof Florida’s Grid for Extreme Weather” available on https://www.fleetcarma.com/electric-vehicles-future-proof-floridas-grid-extreme-weather/ (accessed on May 22,2019).

Gallucci, M., (2018), “Rebuilding Puerto Rico's Grid”, IEEE Spectrum, vol. 55, no. 5, pp. 30-38.

Galvin electricity initiative, (2018), available on “http://galvinpower.org/resources/library/fact-sheets-faqs/electric-power-system-unreliable “(accessed on March 15, 2019)

Gholami, A., Shekari, T., Aminifar, F., Shahidehpour, M., (2016), “Microgrid Scheduling with Uncertainty: The Quest for resilience” IEEE Transactions on Smart Grids, vol. 7, no. 6, pp. 2849-2858.

Hurricane Harvey Event Analysis report by ERCOT, (2017), available on “http://www.ercot.com/content/wcm/lists/144927/Hurricane_Harvey_Event_Analysis_Report.pdf” (accessed on March 5, 2019).

Hurricane HARVEY, (2017), Catholic Sun,” Catholic groups are mobilizing to help in hurricane Harvey’s aftermath” available on http://www.catholicsun.org/2017/08/28/catholic-groups-are-mobilizing-to-help-in-hurricane-harveys-aftermath/ (accessed on November 8,2018)

Hurricane MARIA, (2017), available on http://fortune.com/2017/09/30/donald-trump-blames-puerto-rico-hurricane-maria/ (accessed on November 8,2018)

Jahromi, A., Firuzabad, F., Abbasi, E., (2009), “An Efficient Mixed Linear Formulation for Long -Term Overhead Lines Maintenance Scheduling in Power Distribution Systems”, IEEE Transactions on Power Delivery, vol. 24, no 4, pp. 2043-2053.

Jin, T., Mai, N., Ding, Y., Vo, L., Dawud, R., (2018), “Planning for Distribution Resilience under Variable Generation”, IEEE Green Technologies Conference (Green Tech), 4-6th April 2018, Austin, TX, USA.

Kuntz, A.P., Christie, D.R., Venkata, S.S., (2002), “Optimal Vegetation Maintenance Scheduling of Overhead Electric Power Distribution Systems”, IEEE Transactions on Power Delivery, vol. 17, no. 4, pp. 1164-1169.

L. Xu, (2008),“Underground assessment phase 3 report Ex Ante cost and benefit modeling,” , available: http://www.feca.com/PURCPhase3FinalReport.pdf (accessed on January 10,2018)

Lainfiesta, M., Zhang, X., Sunday, R., (2018),” Design of solar Powered microgrid at Texas A&M University Kingsville”, IEEE Texas Power and Energy Conference (TPEC), 8-9th February 2018, College Station, TX, USA.

Landegren, F., Johansson, J., Samuelsson, O., (2016), “A method for assessing Margin and Sensitivity of Electricity Networks with respect to repair system resources”, IEEE Transactions on Smart Grids, vol. 7, no. 6, pp. 2880-2889.

Li, Z., Shahidehpour, M., Aminifar, F., Alabdulwahab, A., Turki, Y., (2017), “Networked Microgrids for Enhancing Power system resilience”, Proceedings of the IEEE, vol. 105, no. 7, pp. 1289-1310.

Liu, X., Shahidehpour, M., Li, Z., Liu, X., Cao, Y., Bie, Z., (2017), “Microgrids for Enhancing Power Grids Resilience in Extreme Conditions”, IEEE Transactions on Smart Grid, vol. 8, no. 2, pp. 589-597.

Ma, S., Su, L., Wang, Z., Qiu, F., Guo, G., (2018), “Resilience Enhancement of Distribution grids against Extreme Weather Events”, IEEE Transactions on Power Systems, vol. 33, no 5, pp. 1442-1451.

Maharajan, S., Zhang, Y., Gjessing, S., Ulleberg, O., Elliassen, F., (2015), “Providing Microgrid Resilience during Emergencies using Distributed Energy Resources”, IEEE Globecom Workshops (GC Wkshps), 6-10th December 2015, San Diego, CA, USA.

Mathew, R., Ashok, S., Kumaravel, S., (2016), “Resilience assessment in Microgrids using Radial Distribution Network”, IEEE 7 th Power India International Conference (PIICON), 25-27th November 2016, Bikaner, India.

Mensah, F., Dueñas-Osorio, L., (2016), “Efficient resilience assessment framework for electric power systems affected by hurricane events,” Journal of Structural Engineering, vol. 142, no. 8.

Modern power grid, (2019), available on “https://www.researchgate.net/figure/2-Modern-power-grid-intelligently-deploying-DERs-and-renewable_fig1_321134561” (accessed on March 11, 2019).

Mohagheghi, S., Parkhideh, B., Bhattacharya, S., (2012), “Inductive Power Transfer for Electrical Vehicles-Potential Benefits for the Distribution Grid,” IEEE International Electrical Vehicle Conference, 4-8th March 2012, Greenville, SC, USA.

NERC Hurricane Harvey Event Analysis Report available on “https://www.nerc.com/pa/rrm/ea/Hurricane_Harvey_EAR_DL/NERC_Hurricane_Harvey_EAR_20180309.pdf” (accessed on March 11, 2019).

NERC Hurricane Irma Event analysis report available on “https://www.nerc.com/pa/rrm/ea/Hurricane_Irma_EAR_DL/September%202017%20Hurricane%20Irma%20Event%20Analysis%20Report.pdf “(accessed on March 5, 2019)

Panteli, M., Mancarella, P., (2015), “The grid: stronger, bigger, smarter?” IEEE Power and Energy Magazine, vol. 13, no. 3, pp. 58-66.

Panteli, M., Trakas, N.D., Mancarella, P., Hatziargyriou.D.N., (2016), “Boosting the Power Grid Resilience to Extreme Weather Events Using Defensive Islanding”, IEEE Transactions on Smart Grid, vol. 7, no. 6, pp. 2913-2922.

Performance Reviews of EDC’s in 2011 Major Storms by Emergency Prepared Partnerships available on “https://www.nj.gov/bpu/pdf/announcements/2012/stormreport2011.pdf “(accessed on March 5, 2019).

Peter, V., Lawrence., (1995),” Prediction of Hurricane Wind Speeds in the United States”, Journal of Structural Engineering New York, vol. 121, no. 11, pp. 1691-1699.

Pirvault, N., (2013),” Understanding Markov Chains: Examples and Applications”, Springer Publications.

Rahimi, K., Davoudi, M., (2018), “Electric Vehicles for Improving Resilience of the Distribution Systems”, Sustainable Cities and Societies, vol. 36, pp. 246-256.
SAE International, (2018), titled “Standard Collections” available on https://www.sae.org/standards/ (accessed on May 24,2019).

Shin, H., Baldick, R., (2017), “Plug in Electric Vehicle to Home(V2H)- Operation under a Grid Outage”, IEEE Transactions on Smart Grids, vol. 8, no. 4, pp. 2032-2041.

Siever, M., Miller, A., Tauritz, D., (2007),” Blueprint for Iteratively Hardening Power Grids Employing Unified Power Flow Controllers”, IEEE International Conference on Systems of Systems Engineering, 16-18th April 2007, San Antonio, TX, USA.

Smith, A. B., (2018), “2017 US billion dollar weather and climate disasters: a historic year in context”, ClimateWatch Magazine available on https://www.climate.gov/news-features/blogs/beyond-data/2017-us-billion-dollar-weather-and-climate-disasters-historic-year, (accessed on Oct 29, 2018)

Tesla Superchargers available on “https://en.wikipedia.org/wiki/Tesla_Supercharger” (accessed on April 23,2019).

USGS, (2018), “Introduction to National Seismic Hazard Maps” available on https://earthquake.usgs.gov/hazards/learn/ (accessed on Oct 5,2018)

USGS, (2018), “ The Modified Mercalli Intensity Scale” available on https://earthquake.usgs.gov/learn/topics/mercalli.php (accessed on Oct 8,2018).

USGS, (2018), “Earthquake Hazards Programs available on “https://earthquake.usgs.gov/hazards/learn/basics.php “(accessed on August 10,2019).

Wang, Y., Chen, C., Wang, J., Baldick, R., (2016), “Research on Resilience of Power Systems Under Natural Disasters—A Review”, IEEE Transactions on Power Systems, vol. 31, no. 2, pp. 1604-1613.

Yao, S., Zhao, T., Wang, P., Zhang, H., (2017), “Resilience oriented Distribution system reconfiguration for service restoration considering distributed generations”, IEEE Power and Energy Society General Meeting, 16-20th July 2017, Chicago, USA.